frontiers | Frontiers in Earth Science

TYPE Original Research
PUBLISHED 21 October 2024
DOI 10.3389/feart.2024.1475025

Check for updates

OPEN ACCESS

EDITED BY
Pier Paolo Bruno,
University of Naples Federico II, Italy

REVIEWED BY
Emanuele Lodolo,
National Institute of Oceanography and Applied Geophysics, Italy
Anna Gabàs I Gasa,
Institut Cartogràfic i Geològic de Catalunya, Spain

*CORRESPONDENCE
Denis Anikiev,
denis.anikiev@gfz-potsdam.de

RECEIVED 02 August 2024
ACCEPTED 30 September 2024
PUBLISHED 21 October 2024

CITATION
Götze H-J, Strehlau R, Dannowski A, Anikiev D, Kumar A and Scheck-Wenderoth M (2024) Do gravity data justify a rifted "Liguro-Provençal Basin"?
Front. Earth Sci. 12:1475025.
doi: 10.3389/feart.2024.1475025

COPYRIGHT
© 2024 Götze, Strehlau, Dannowski, Anikiev, Kumar and Scheck-Wenderoth. This is an open-access article distributed under the terms of the Creative Commons Attribution License (CC BY). The use, distribution or reproduction in other forums is permitted, provided the original author(s) and the copyright owner(s) are credited and that the original publication in this journal is cited, in accordance with accepted academic practice. No use, distribution or reproduction is permitted which does not comply with these terms.

Do gravity data justify a rifted "Liguro-Provençal Basin"?

Hans-Jürgen Götze[1], Ronja Strehlau[1], Anke Dannowski[2], Denis Anikiev[3]*, Ajay Kumar[3,4] and Magdalena Scheck-Wenderoth[3,5]

[1]Institute of Geosciences, Kiel University - Christian-Albrechts-Universität zu Kiel, Kiel, Germany, [2]GEOMAR - Helmholtz Centre for Ocean Research Kiel, Dynamics of the Ocean Floor, Divison 4, Kiel, Germany, [3]Helmholtz Centre Potsdam – GFZ German Research Centre for Geosciences, Section 4.5 – Subsurface Process Modelling, Potsdam, Germany, [4]Department of Earth and Climate Science, Indian Institute of Science Education and Research, Pune, India, [5]Faculty of Georesources and Material Engineering, RWTH Aachen University, Aachen, Germany

The geodynamic evolution of the Liguro-Provençal Basin and its crust and upper mantle structure remain debated, especially regarding the role of rifting in continental break-up and seafloor spreading. Our study incorporates updated datasets, including new gravity maps from the AlpArray Gravity Working Group (complete Bouguer, free air, and isostatic anomalies) for 3D modeling and gravity field analysis, seismic data from Lobster offshore campaigns for direct comparison, and geodynamic models, supplemented by seismic profiles from previous French and Italian campaigns to constrain the interpretation. We used GFZ's IGMAS + software for interactive 3D modeling, creating a density model extending to 300 km depth that includes crustal and upper mantle inhomogeneities based on prior geodynamic models. This hybrid approach, with polygonal structures for the crust and voxels for the upper mantle, clarifies individual contributions to the gravity field. Extending initial gravity modeling from the SPP MB4D project INTEGRATE, our work provides a consistent 3D density model for the Alps and Ligurian Basin. The constrained 3D modeling and numerical analyses (terracing, clustering, filtering, curvature), along with vertical stress and gravitational potential energy calculations, suggest that rifting has significantly influenced the basin's geological evolution.

KEYWORDS

AlpArray gravity map, Liguro-Provençal Basin, Bouguer anomaly, potential field processing, residual gravity, mediterranean lithosphere

1 Introduction

The work presented here is part of two European initiatives: the AlpArray initiative (Hetényi et al., 2018) and the German Priority Program (SPP 2017) "Mountain Building in 4D" (e.g., Handy et al., 2014). In our study, 3D gravity modeling is used to elucidate the lithosphere structure in the Liguro-Provençal Basin, located in the northwestern Mediterranean.

Due to the static nature of recent gravity fields, dynamic and evolutionary geological questions cannot be directly addressed. Instead, we focus on the following key questions:

- Crustal architecture and tectonic evolution: What is the density of the crust beneath the Liguro-Provençal Basin, also referred to as the "Sardo Provençal Basin" by Morelli et al. (2022)?
- Rifting and continental break-up: Did rifting processes create areas with different density domains in the crust? Did rifting lead to continental break-up, and can we identify the transition between continent and ocean?
- Moho depth and crustal thickness: What is the boundary between the crust and mantle in the Liguro-Provençal Basin?

We investigate these key points through the lens of gravity anomalies and their relationship to crustal structure. Our study demonstrates how three-dimensional density modeling can help address these questions. Due to the inherent ambiguity in interpreting gravity fields, this approach is only valuable when supported by independent information and data (constraints). These constraints are primarily obtained from active seismic experiments and seismicity catalog data in the Liguro-Provençal Basin.

A notable feature of our modelling is the comparison of our results with the modern compilation of the AlpArray Gravity Research Group (AAGRG, Zahorec et al. (2021)) of the gravity field in the Alpine-Mediterranean region. We integrate gravitational potential energy and vertical stress analyses to obtain insights into the distribution of forces associated with the gravity field. With this approach we try to link gravity field analysis with geodynamic interpretations, which often differ from interpretations of static fields such as gravity.

Note: All gravity field values in the text are given in mGal and the corresponding SI units.

2 Geological framework

The northwestern Mediterranean Sea has been the target of numerous national and international research campaigns.

The Liguro-Provençal Basin is located in the northeastern part of the Western Mediterranean Basin (Figure 1). It is a back-arc basin that developed during the Oligocene and Miocene (Le Breton et al., 2021) caused by the southeast rollback of the Apennines-Calabrian subduction zone (Jolivet and Faccenna (2000). Below the Liguro-Provençal Basin, the Moho depth varies ranging from about 12 km southwest of Sardinia to 20 km southwest of Genoa, reaching depths of about 30 km beneath Sardinia, Corsica, and the northwestern basin margins (e.g.; Rollet et al., 2002; Gailler et al., 2009; Dannowski et al., 2020; Wolf et al., 2021; Canva et al., 2021; Makris et al., 1999). The sedimentary cover in the Liguro-Provençal Basin is thickest between the Gulf of Lion and Sardinia, where it attains up to 8 km, decreasing northeastward to about 3–4 km offshore Genoa (Schettino and Turco, 2006).

Rifting in the region between France and Sardinia began about 32 million years ago (Vigliotti and Langenheim, 1995), in response to extension initiated by the rollback of the Calabrian-Apennine subduction zone. Subsequently, the Corsica-Sardinia block and the bordering oceanic crust began to rotate counterclockwise between 21 and 15 million years before present (Siravo et al., 2023). The magnitude of this rotation is estimated to be between 23° and 53°, with various studies providing different estimates: ~23° during Miocene times (Speranza et al., 2002), 30° (Vigliotti and Langenheim, 1995), 45° (Gattacceca et al., 2007), and ~53° during Oligocene-Miocene times (Le Breton et al., 2017). About 16 million years ago, both the rotation and the rifting of the basin ceased when the Apennine Mountains halted the movement of the Corsica-Sardinia block (Rosenbaum et al., 2002). Subsequently, extension continued east of Corsica-Sardinia, leading to the opening of the Tyrrhenian Sea (Le Breton et al., 2017). Whether the rifting only caused thinning of the crust within the basin or led to the formation of new oceanic crust remains unclear, with suggested timing of tectonic phases differing among various authors (e.g., Barruol et al., 2004; Jolivet et al., 2020).

Asch (2005) defined five main geological units in the Liguro-Provençal Basin (Figure 1B): Unit 1: Oceanic crust, extending from offshore northwest of Corsica in a southwesterly direction, past Sardinia. This assertion contrasts with findings derived from seismic profiles of the region, that indicate only continental crust below the Ligurian Basin (Dannowski et al., 2020). Unit 2: Transitional crust (e.g., Gailler et al., 2009) or serpentinized mantle (Merino et al., 2021) surrounded by continental crust (unit 3). The thinned continental crust (unit 2) forms an envelope around unit 1, with a small extent in the southern part and a wider extent in the northern part. Unit 3: undifferentiated continental crust. Unit 4: Intrusions of igneous rocks, mostly occurring within unit 2, covering near-coastal regions offshore Barcelona and offshore Corsica and Sardinia. Unit 5: Ophiolites, remnants of the Tethys Ocean, located in the north of Corsica and in the northeastern Liguro-Provençal Basin.

3 Potential field database

Understanding the gravity field anomalies in the Alpine-Mediterranean region has several important implications for various fields of research and practical applications. In the following sections, we will briefly highlight these.

3.1 Past and present gravity databases

The first Bouguer gravity map for the entire Mediterranean region, published by Makris et al. (1999), was a milestone.These data have been acquired starting from the beginning of the 60 s, and from today's perspective, the numerical methods used for data processing did not meet modern methodological requirements. The old Bouguer gravity map by Makris et al. (1999) is shown in Figure 2A. It has a large scale, is of lower resolution and unsuitable for resolving short wavelength anomalies, which are important for modeling purposes.

The new gravity field compilations published by the "AlpArray Gravity Research Group, AAGRG" (Zahorec et al., 2021) on a 4 km × 4 km grid for both Bouguer and Free air anomalies provide a database suitable for 3D modeling (Figures 2B, 3). These compilations follow the most recent gravity processing standards. After removing long wavelength regional fields, the gravity map shows local structures valuable for modeling shallow density variations in the subsurface. The Bouguer anomalies are

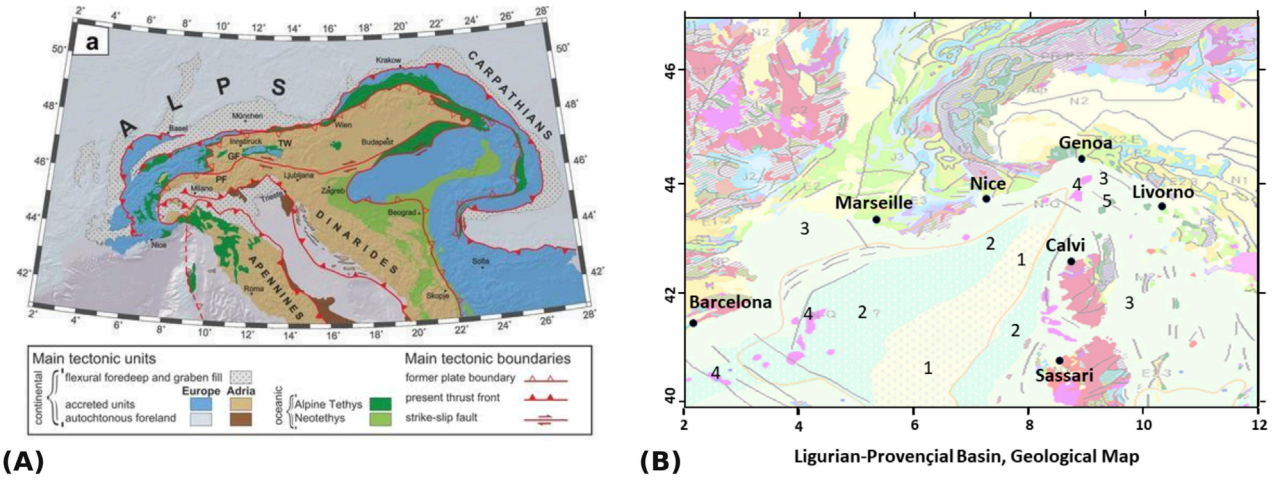

FIGURE 1
Study Area of the SPP MB-4D in the Alps and Surroundings: **(A)** The main tectonic units of the Western and Eastern Alps, the Dinarides, the Apennines, and the Carpathians, along with their key features. Green colors indicate oceanic areas, while blue and brown colors indicate continental units. PF - Periadriatic Fault, a major late orogenic fault system offset by the Giudicarie Fault (GF). TW - Tauern Window. Map from Hetényi et al. (2018). **(B)** Submarine geological units (IGME 5000, after Asch (2005)): unit 1 - Oceanic crust formed during rifting in the area, unit 2 - Thinned continental crust stretched during rifting, unit 3 - undifferentiated continental crust, unit 4 - Intrusions of igneous rocks and 5: Ophiolites.

complete (CBA) and generated using the latest criteria and reference frames (both positional and gravity reference systems). Atmospheric corrections were also applied. Error statistics (Zahorec et al., 2021) based on cross-validations and interpolation residuals indicate high data accuracy. For example, the Austrian dataset shows interpolation residuals between −8 and +8 mGal, cross-validation residuals between −14 and +10 mGal, with standard deviations well below 1 mGal. The database accuracy is approximately ± 5 mGal for most areas. This compilation shows negative gravity values in the Alps and the Po Basin in northern Italy. The Ivrea high in the western Italian Alps and the dominant high in the Bouguer anomaly in the Liguro-Provençal basin are clearly visible. Detailed descriptions of individual anomalies can be found in Zahorec et al. (2021).

3.2 Bouguer anomaly

The Bouguer anomaly map (Figure 3A) features positive anomalies offshore and moderate to negative values on land. Bluish colors indicate strong negative gravity in the Apennines, the Po Basin, and the Southern Alps, reflecting crustal root density deficits. A significant advancement of this compilation is its resolution, showing short wavelengths even in the offshore region of the Liguro-Provençal Basin, Corsica, and northern Sardinia. The effects of the Ivrea body and previously unknown positive anomalies in the Liguro-Provençal remain in the residual field. In Corsica, the anomalies are significantly smaller than in the offshore Mediterranean Sea. Detailed information on calculating the CBA by filtering/smoothing is provided in the text.

For the gravity field interpretation presented in Section 6, it is still necessary to eliminate a regional field from the CBA. The following procedure was used: 1) subtraction of the XGM 2019e_2159 satellite field (ICGEM website, http://icgem.gfz-potsdam.de/tom_longtime), 2) slight spline smoothing to eliminate remaining small local artifacts. The resulting residual field at the end of this procedure is referred to here and later as the "residual field" (Figure 3B).

3.3 Free air anomaly

In addition to the new Bouguer map, a Free air anomaly map has been compiled by the AAGRG (Zahorec et al., 2021). This new map provides more details than previous compilations for the region (e.g., Sandwell et al., 2014).

Although most gravimetric models use Bouguer gravity fields as the reference, we chose free air anomalies (Figure 3C) to be compatible with the previous 3D density model for the Alps and their forelands - 3D ALPS (Spooner et al., 2019b; Spooner et al., 2019a), which uses Free air anomalies and was available for our studies. This approach allows the inclusion of rock-related density inhomogeneities in the crust between the surface and the model reference level. Our goal was to extend the 3D ALPS model to the offshore Ligurian Sea, ensuring compatibility with the existing density model of the Alps.

As expected, the image of the Alpine Free air anomalies is strongly influenced by the topography of the study area: gravity highs largely correlate with high topographic elevations (Western Alps, Apennines, Corsica, etc.), while extended lows indicate lower density in the Po basin of northern Italy. Deviations suggest density changes in the Earth's crust and lithosphere. For the 3D model calculations, also the Free air anomaly of the AAGRG was smoothed, as a detailed 3D gravity model using the original Free air anomaly would have been too large in terms of model size and the number of gravity stations to process for interactive modeling (both storage and computation time).

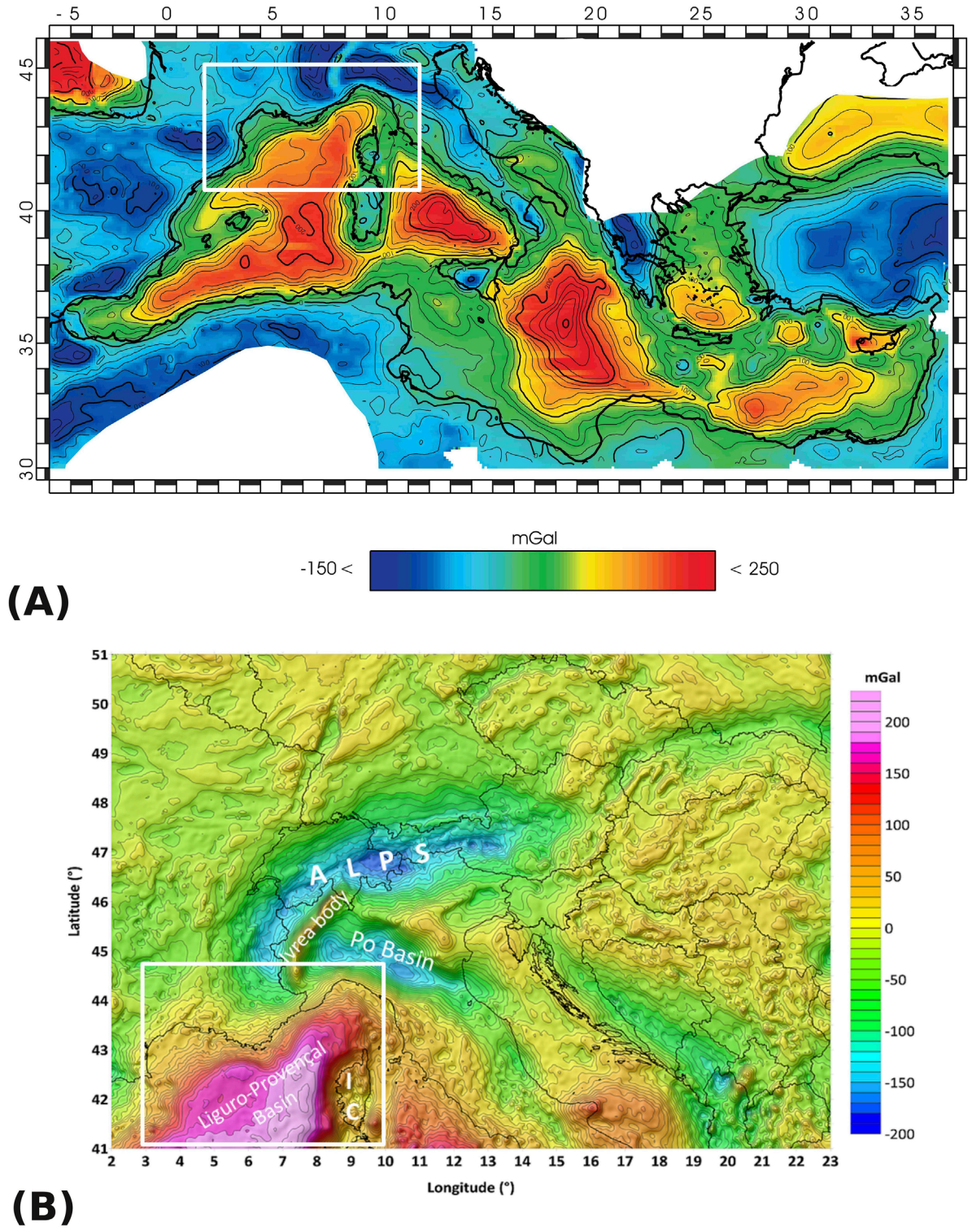

FIGURE 2
The Bouguer gravity map of the Liguro-Provençal Basin/Western Mediterranean according to Makris et al. (1998) **(A)**. The isoline distance is $10 \times 10^{-5} m/s^2$ (10 mGal) at a scale of 1: 1 million. From today's perspective, the ship gravimetry processing does not meet modern standards and is rough and erroneous in some areas. The white rectangle marks our study area. **(B)** The new AlpArray Bouguer gravity map of the Alps and adjacent areas. The white box in the southwest indicates the modeled area in this paper. IC = Isle of Corsica. The black lines represent political boundaries on land and the coastline of the Mediterranean Sea with Corsica and northern Sardinia.

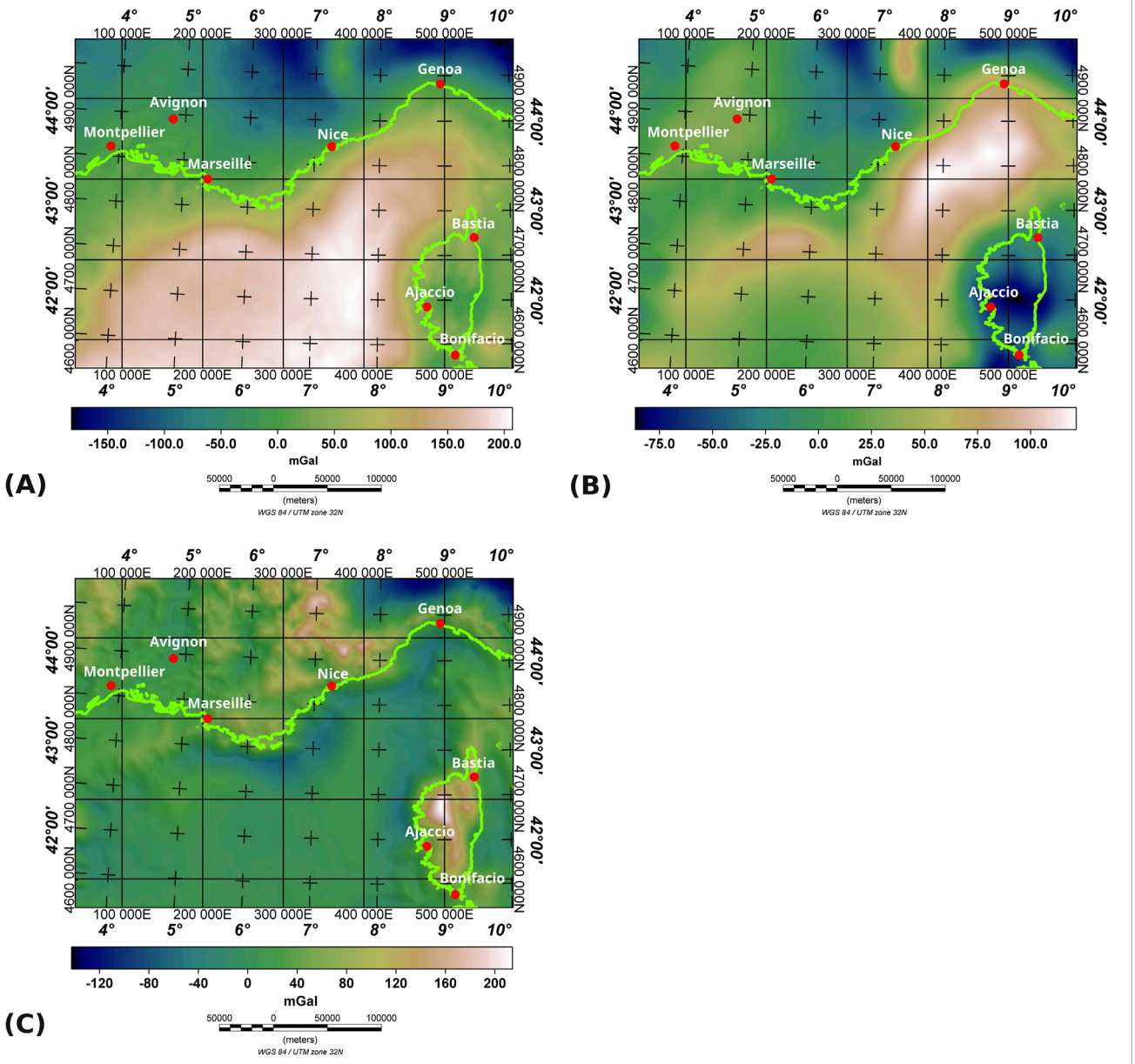

FIGURE 3
Gravity maps with the coasts marked with green lines (A and B from Zahorec et al. (2021)). **(A)** Bouguer anomaly: The new AAGRG Bouguer gravity map of the Liguro-Provençal Basin/Western Mediterranean. This map is based on a $4km \times 4km$ grid of the complete CBA map. CBA stands for "complete Bouguer anomaly". **(B)** The residual field of the complete Bouguer anomaly (CBA) after elimination of regional anomalies that would hinder the interpretation in the local area of the Liguro-Provençal Basin. **(C)** Free air anomaly: compiled by the AAGRG for the Alps and their foothills. On land, the Free air anomaly follows the topography of the surface. Offshore, in the Liguro-Provençal Basin, significant gravity differences can also be observed due to uneven bathymetry.

4 Modeling and data constraints

Due to the ambiguity inherent in potential field interpretation, constraining data is required for accurate modeling. The most important constraints for our density modeling come from seismic imaging methods, using both refraction and reflection data, as well as information from passive seismic data sets. Additionally, we compare our modeled Moho with the regional compilation of the European Moho (Grad et al., 2009). This digital Moho depth map is based on over 250 seismic profiles, several 3D models, body and surface waves, and receiver functions, with gravity data added in selected areas. European Moho data are shown in green in all corresponding model depth sections (e.g., Figures 8A, 9).

4.1 Refraction and reflection seismic data

Considerable interest has focused on studying the lithosphere of the western Mediterranean using seismic methods. An overview of campaigns in the Liguro-Provençal Basin up to 2002 is provided by

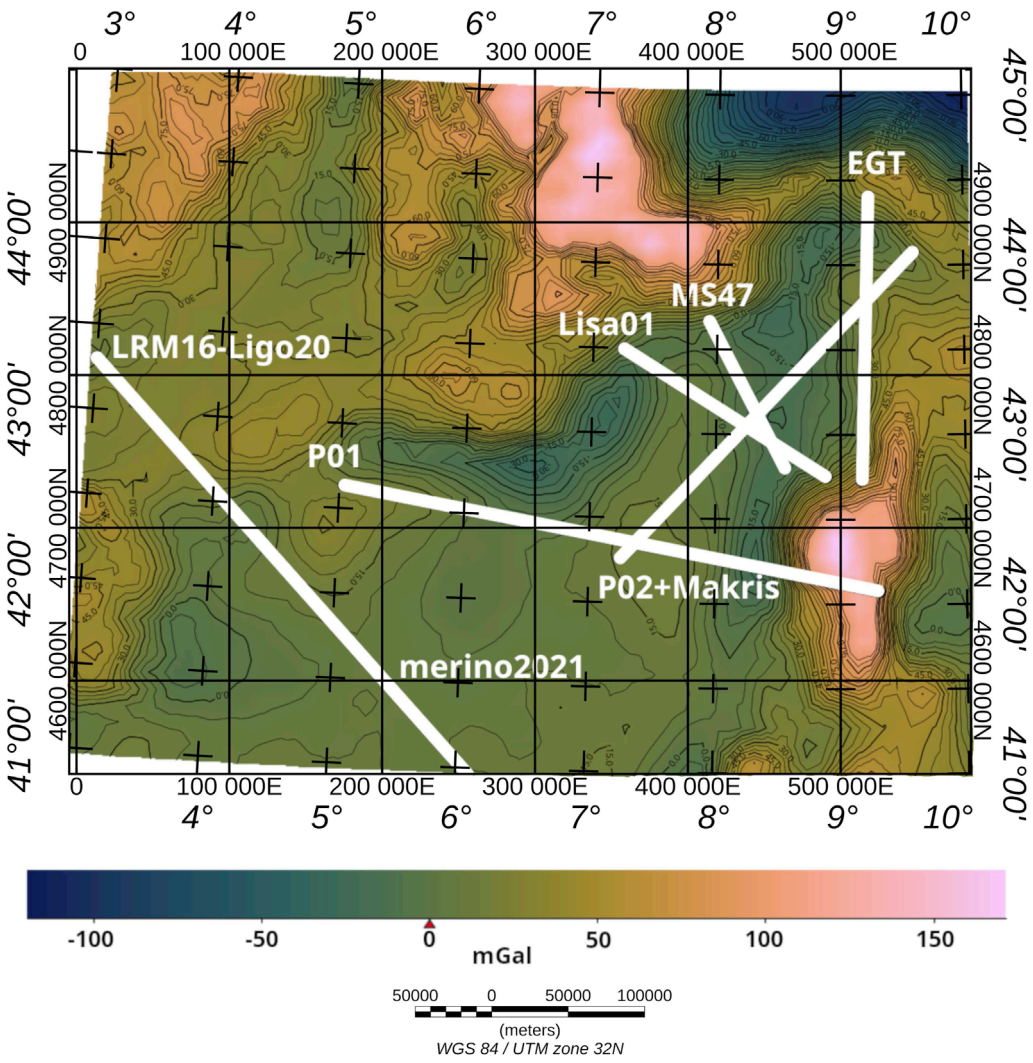

FIGURE 4
Location of the georeferenced seismic profiles used to constrain the model over the Free air anomaly map. P01 (Dannowski et al., 2020) and P02+Makris (Dannowski et al., 2020; Makris et al., 1999); merino 2021 (Merino et al., 2021), EGT (Ginzburg et al., 1986), LISA01 (Contrucci et al., 2001) and M S47 (Finetti and Morelli, 1973) are the main profiles shown in detail in Figures 8A,B below.

Rollet et al. (2002). Recent surveys include the CROP deep seismic profiles (De Voogd et al., 1991; Finetti and Morelli, 1973), TGS-NOPEC and SARDINIA profiles (Gailler et al., 2009; Jolivet et al., 2015), the GROSMarin 3D seismic refraction project (Dessa et al., 2011), the LOBSTER campaign (Dannowski et al., 2020; Kopp et al., 2023), and the SEFASILS cruise (Dessa et al., 2020). These studies, along with other gravimetric and geological data, serve as important constraints for our gravity modeling. See Figure 4 for the location of seismic lines used to constrain our density model.

Other important constraints for our 3D density modeling come from earlier shipboard seismic measurements by Makris et al. (1998) and measurement campaigns by Morelli and colleagues (e.g., Morelli and Nicolich, 1990; Morelli et al., 1975), which provide insights into the lithosphere structure in the western Mediterranean. Due to the early stage of density modeling development at the time, the density models of these authors in the Ligurian Sea are relatively simple.

4.2 Passive seismic data

Figure 5 shows earthquake distribution in the Ligurian Basin, based on the USGS earthquake catalog (U.S. Geological Survey, 2021). Events between January 1900 and February 2021 with a minimum magnitude of Mw 2.5 are included, with the largest earthquakes reaching magnitudes up to Mw 6.5 at the Ligurian margin. Earthquakes are divided into shallower, 5–20 km deep (yellow/orange), and deeper than 50 km (dark violet) focal depths in Figure 5.

Within the Liguro-Provençal basin, no events deeper than 50 km were observed. On the Italian mainland, especially southeast of Genoa, many earthquakes occur at depths of 10–20 km due to the subduction of the Adriatic plate Doglioni et al. (1999). A cluster of earthquakes of magnitude 2.5 is located in the NW Liguro-Provençal Basin. A notable feature at 42°N and 7.0° to 7.5°E is the accumulation of earthquakes with epicenters in

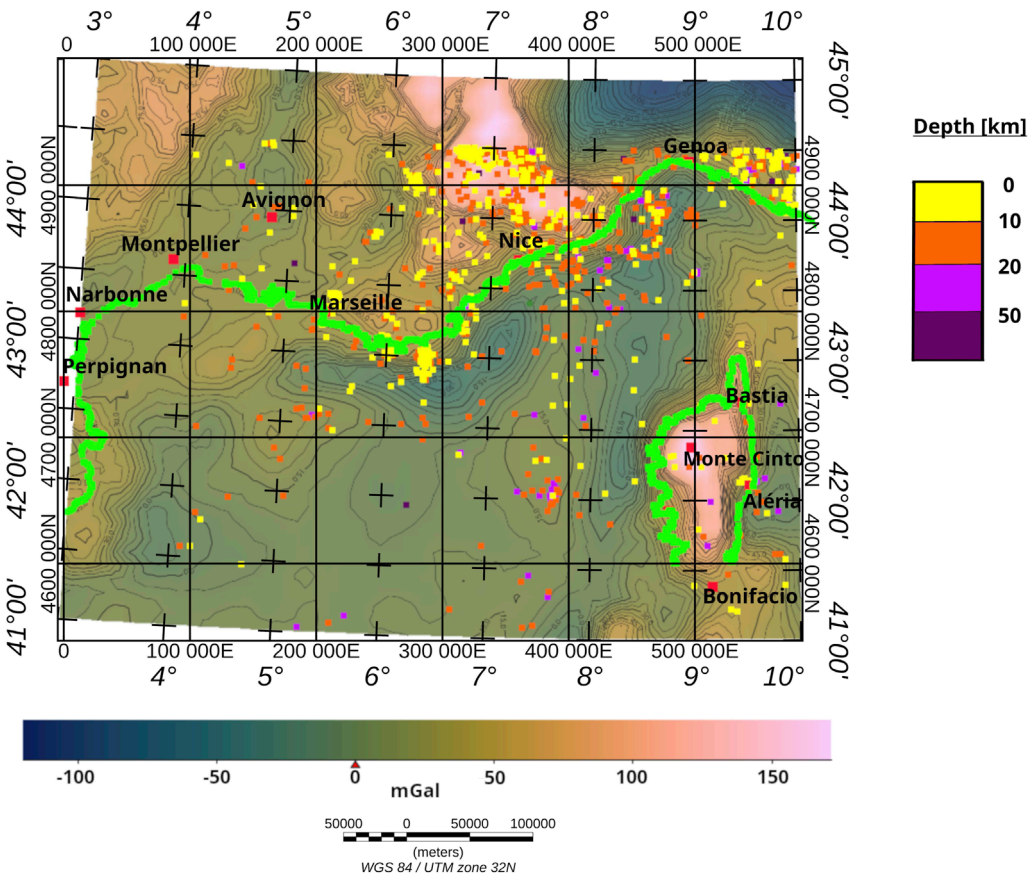

FIGURE 5
Distribution of earthquake epicenters with magnitude 2.5 and higher in the region at depths between 0 and 100 km (U.S. Geological Survey, 2021) superimposed on the Free air anomaly. The northern part of the Ligurian basin has a higher density of earthquakes. Earthquakes occur more frequently in the central area where Free air and Bouguer anomalies display elevated values compared to other parts of the basin.

depths between 10 and 50 km (orange and pink). Thorwart et al. (2021) interpreted this cluster and the focal mechanisms as an indication of "re-activated pre-existing rifting-related" structures. This cluster corresponds spatially with steep gradients in the gravity field of the upper mantle, as shown in Figures 5, 15. Several amphibious ambient noise studies have been conducted in the region (Guerin et al., 2019; Wolf et al. (2021); Nouibat et al. (2021)). From these observations the 3D group velocities were used to calculate 1D depth inversion for S-wave velocities. The results show that the Moho drops from 12 km below the southwestern center of the Liguro-Provençal basin to 20–25 km below the Ligurian coast in the northeast and to over 30 km depth near the coast of Provence.

5 Gravity data processing and 3D modeling

This section outlines the gravity field processing and modeling methodology and presents the obtained results. Detailed interpretation is provided in Section 6.1.

5.1 Curvature

Curvature computation has become prominent in geophysics since Roberts (2001). In potential field interpretation, curvature is used to enhance the identification and delineation of subsurface geological structures such as edges of density (or magnetization) contrasts. Its attributes in both seismic and potential methods offer deeper insight into the geometry of the corresponding distributions (e.g., velocity, gravity and magnetic fields). Ebbing et al. (2018) and Li (2015) demonstrated how gravity gradients from recent satellite missions support the interpretation of regional to global gravity fields. However, for our local study, satellite data resolution was insufficient for interpreting laterally rapidly changing structures. Instead, we used the in-house software curvature by Dr. Sabine Schmidt to analyze residual fields processed from Bouguer anomalies (Figure 3C). Free-air and Bouguer anomalies can be used equivalently if the topographic reduction in the Bouguer anomaly accounts for the actual density distribution of the masses between the surface and the reference level. In the case of the free-air anomaly, the effect of these inhomogeneities is still present in the field and must therefore be included in the

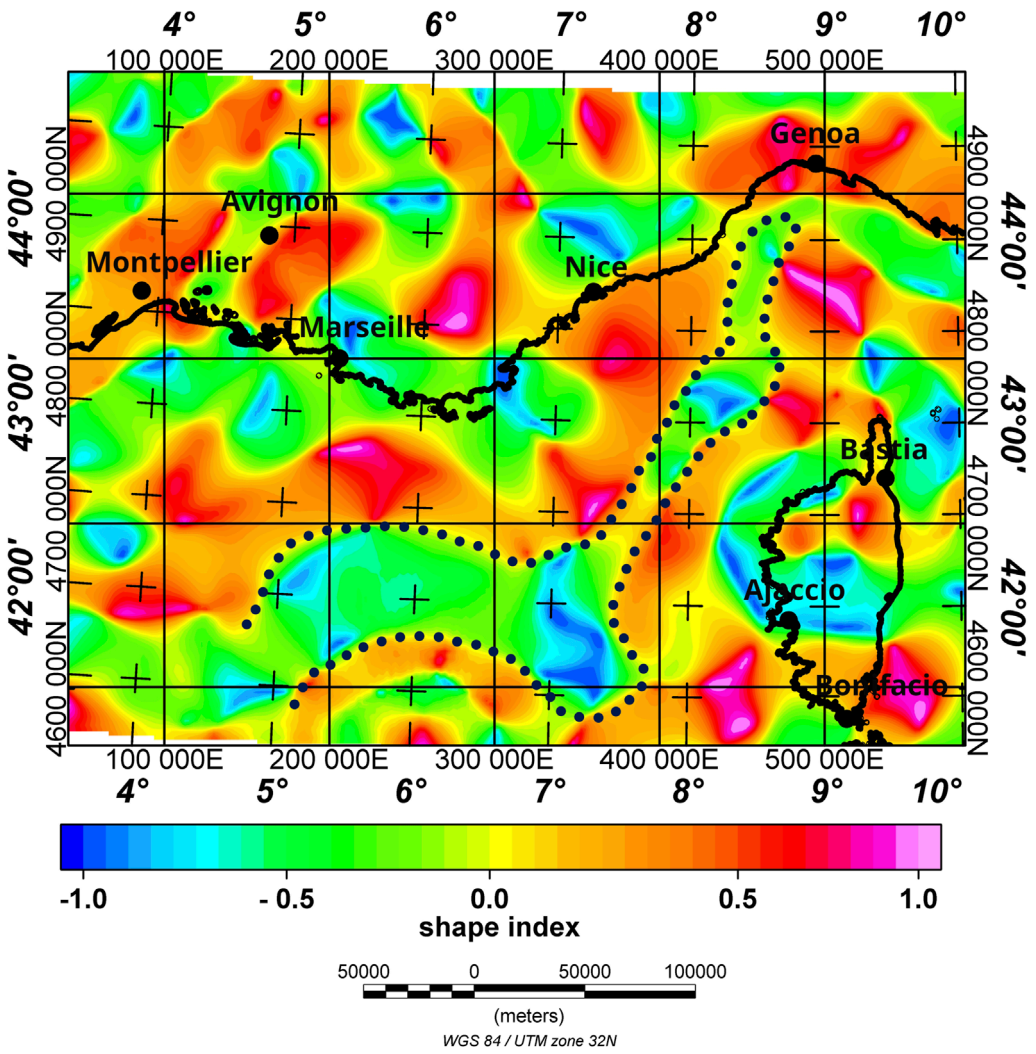

FIGURE 6
Shape curvature calculation of the residual field in Figure 3B. Red tones visualize "ridge-like" structures with high shape indices, some having local maxima (magenta). Blue-green shades indicate areas of lower shape indices ("valleys" or "lows" as per Roberts (2001)). The dotted line encloses an area where the curvature exhibits a "valley character" in the central Ligurian Sea.

modeling. Figure 6 shows the "indices of shape curvature" of the residual field (Figure 3B), distinguishing between convex, concave, flat, and ridge manifestations and correlating them with geological structures. Different colors indicate typical shape characteristics: valleys (blue to green), flat areas (yellow), ridges (orange to red), and dome-like convexities (magenta).

The overall shape index picture is complex, but a narrow band with "valley characteristics" (green-blue colors) in the center of the Ligurian Basin can be identified between high elevations off the French Mediterranean coast and Corsica (yellowish and red colors). This contrast may indicate a narrow rift zone, a hypothesis explored further in Section 6.

5.2 Terracing and clustering

Terracing and clustering identify patterns, anomalies, and structures in the Earth's subsurface based on gravity field variations. Both methods were prepared for use in the Ligurian Sea by Strehlau et al. (2022). Terracing partitions a gravity anomaly dataset into distinct amplitude or gradient intervals, or "terraces," highlighting variations and aiding in identifying subsurface features, geological boundaries, and density anomalies. Cooper (2020) presented the method, which uses the Laplacian function and has recently been replaced by the potential field shape index. The filtering process iterates until the result provides unique homogeneous segments and the "terracing effect" is visible. For the terraced residual field in Figure 3B, the gravity field in Figure 7A shows a simplified but clearer picture. Reddish colors indicate high residual gravity and green-blue colors indicate low values. The result is similar to the shape curvature analysis, revealing a narrow strip of low gravity in the study area center. Clustering applied to terraced gravity field data uses mathematical algorithms, such as k-means or hierarchical clustering, to group similar gravity anomaly measurements into clusters. These clusters represent regions with analogous gravity anomaly patterns, indicating

underlying geological structures or subsurface phenomena with common density distributions. This method helps to reveal spatial relationships and coherent structures within the data. The number of clusters, k, is specified by the user. Initially, the cluster centers' positions are randomly determined and then optimized using the method of least squares. Further methodological details are described in Florio and Lo Re (2018) and Kodinariya and Makwana (2013). In this study, three clusters (k = 3) were used and applied to the residual field computed from the CBA in Figure 3A. The clustering result is shown in Figure 7B. It highlights a narrow zone of low gravity (cluster 1) in the center of the basin, surrounded by a broader cluster (cluster 2). This result illustrates, like the terracing results, the advantage of cluster analysis in representing terraced distributions, effectively reducing the map to its essential content.

5.3 3D modeling with IGMAS + software

Our forward modeling concept involves interactive fitting of potential fields (Free air anomalies) using IGMAS + (Interactive Gravity and Magnetic Application System), a free software tool with nearly 40 years of development (Anikiev et al., 2021; Anikiev et al., 2023b; Götze et al., 2023). IGMAS + uses an analytical solution of the volume integral for gravity and magnetic effects of homogeneous bodies bounded by polyhedrons of triangulated model boundaries (Götze and Lahmeyer, 1988; Schmidt et al., 2011; Anikiev et al., 2023a). The backbone model is constrained by multidisciplinary data such as geological maps, well data, seismic reflection and refraction profiles, structural signatures from seismic receiver functions, and local surveys. The software supports spherical geometries and optimized memory for fast inversion of material parameters and changes in model geometry. Its highly interactive technique makes IGMAS + user-friendly, operating in real time while preserving model topology. Due to its triangular model structure, IGMAS + handles complex structures (multi-Z surfaces) like overhangs of salt domes well. An inversion tool for automated modeling was recently published (Alvers et al., 2023). This software was used to model the gravity field of the lithospheric subsurface to a depth of 300 km in the Liguro-Provençal Basin. Gravity data and constraints were provided by the datasets described earlier.

5.4 Model description and results

The 3D model's basis was the density distribution in the 3D ALPS model (Spooner et al., 2019b; Spooner et al., 2019a). Model structures from 3D ALPS remained unchanged in the eastern and northern parts and were interactively modified in the southern Liguro-Provençal Basin. 3D views of the model are shown in Figures 8A,B. Due to the complex Alpine density distribution between the land surface and the Bouguer anomaly reference level (0 m), we modeled the Free air anomaly (Figure 3C). The disadvantage is that the model's spatial resolution is sparse, and some details of mountains and model surfaces cannot be represented, especially for Corsica and parts of the French-Italian Alps. Therefore, we truncated the drawing of the Free air anomaly isolines at a certain value. All larger anomaly values appear as pink patches in the maps (e.g., Figures 8A,B, 10A,B). The model is constructed with 33 vertical planes: 31 central planes for modeling and two peripheral planes in the west and east (not shown in Figure 8) to avoid edge effects (e.g., Alvers et al., 2015). The 2.911 model stations were placed on a regular grid with about 7 km spacing (Figure 8A). The reference gravity (Free air anomalies) appears at the top. The lower part of the model (between 50–300 km depth) is represented as a voxel cube, where each voxel is assigned a density value.

In addition to Figure 8A, more model details are shown in Figure 8B. The top surface of the model is hidden, and the stations are turned off. Inside the model, you can see the vertical planes that define the interior and the georeferenced position of the seismic profiles from Figure 4. The perspective view also shows the subsurface structures, indicated by different colors corresponding to model densities in Figure 8C below the model views. Model densities and corresponding colors were used in our model of the Liguro-Provençal Basin which are shown in Figures 8, 9, 11 (after Spooner et al. (2019b); Spooner et al. (2019a)). Note: Density values with six decimal places are calculated by inverting the DENSITY parameter; only the first two digits are significant. The vertical planes (12, 23, 26) will be shown later as examples of the model structure (Figure 9), as well as the seismic profiles P01 and P02 + Makris (Dannowski et al., 2020).

Reliable seismic constraints were available for much of the study area, so the model geometry was not significantly changed, and densities were kept as constant as possible compared to Spooner et al. (2019b)). Free air anomalies were propagated up to 6 km to ensure model stations were always above the model surface, which is up to 3 km for the southern French Alps and 2.7 km for Corsica.

All three model curves in Figure 9 along vertical Sections 12, 23, and 26 in Figure 8B (green/white stippled lines) and 10 (red lines) fit the reference anomaly. This is evident in the residual map below (Figure 10C). Since the 3D ALPS model of Spooner et al. (2019b) was compiled for the Central Alps and the Ligurian Sea margins, we slightly modified the geometry of the geological bodies. Our workflow was to fit the model Moho such that it was consistent with the Moho compilations from seismic campaigns (profiles in Figure 4) and in areas not covered by seismic lines with the Moho of Grad et al. (2009). Then, the geometries of the geological bodies were adjusted, and their densities were changed (inverted) if necessary. Differences between reference and model gravity are mostly less or equal than $5 \times 10^{-5} m/s^2$ (5 mGal).

All densities and corresponding colors in Figure 9 match those in Figure 8C. Section 12, located at the far west of the area, intersects a gravity high offshore of France, followed by another gravity high further south. The first high is attributed to near-surface structures (consolidated sediments), while the second is due to an elevated Moho position. Subsurface structures along vertical Section 23 differ significantly further east. Here, a pronounced, localized gravity high on land (green body, "u crust Apennine," density 2,720 kg/m^3) is bordered by a relative gravity minimum, caused by increasing water depth, the tapering of the 2,720 kg/m^3 body, and the rise in 2,400 kg/m^3 "consolidated sediments." A similar pattern appears in Section 26's gravity profile, east of the previous section. Initially dominated by the high-density 2,720 kg/m^3 body, the profile shows a uniform trend until gravity increases again in the south, due to the higher densities of the Corsica-Sardinia block. Refer to Figure 11 for comparison.

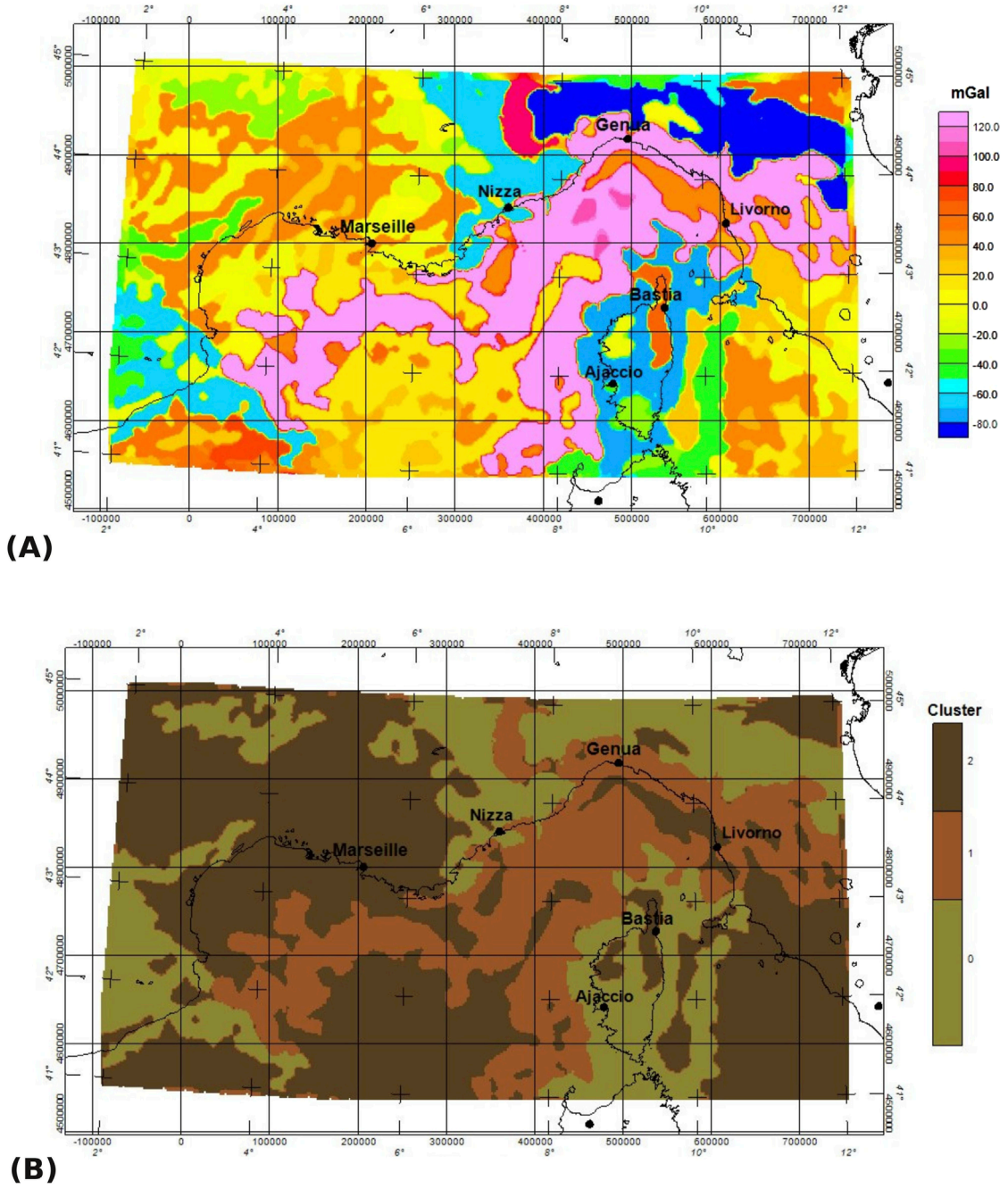

FIGURE 7
Terracing results for the Liguro-Provençal basin and adjacent area **(A)**. Based on Figure 3B with minimum curvature, grid spacing of 2 km, a gamma threshold of 0.1, and 200 iterations applied. The result shows a narrow band (yellow) of low residual gravity surrounded by higher values, similar to shape curvature analysis (Figure 6). **(B)** Clustering results of the terraced Bouguer anomaly fields, showing a narrow band (cluster 2, dark brown) of reduced gravity already shown in Figure 7A.

5.5 Density calculations between 50–300 km depth

The crustal domain in the model is supported by extensive seismic survey data (Figure 4). This is not the case for the upper mantle, whose architecture has recently become better known through the AlpArray Consortium tomography and the 4DMB SPP, but still lacks clarity on whether interpreted plates are consistent with observed surface deformation and topography. For mantle modeling, we relied on Kumar et al. (2022), combining shear wave tomography models into a statistical ensemble to derive three scenarios for plate lithospheric thickness and geometry. These scenarios were used for geodynamic simulations to calculate topography, surface velocities, and mantle flux. The scenario

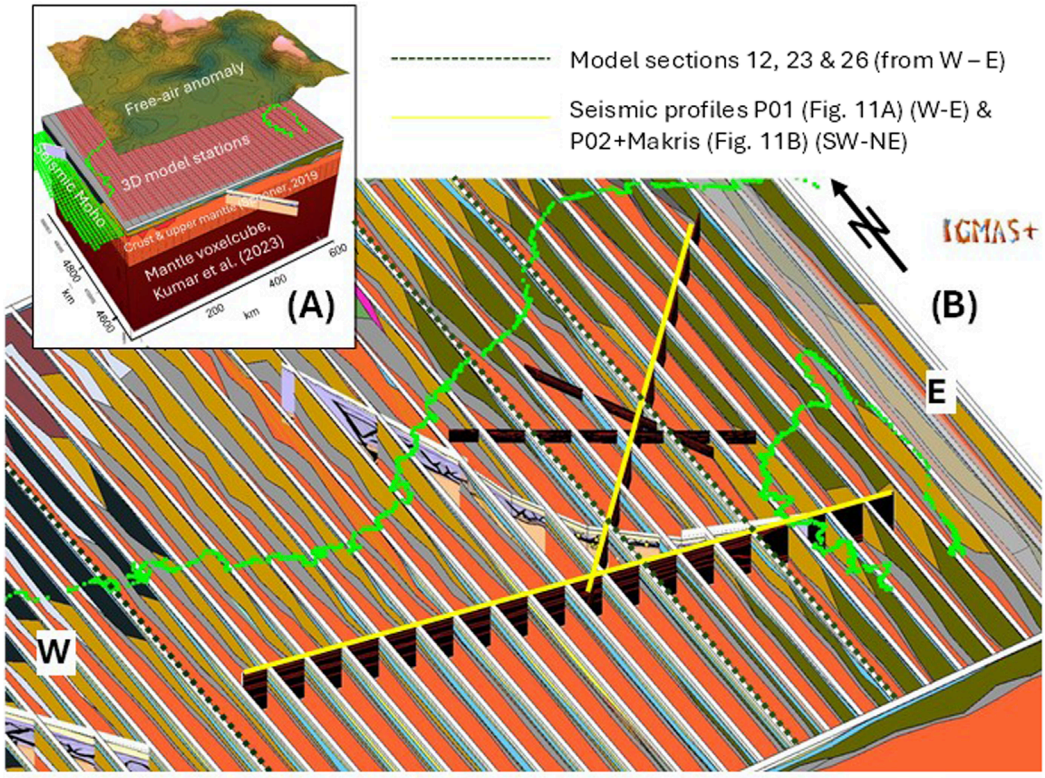

Name	Density[kg/m³]
01_Water	1024.999998
020_Loose_Sed	2200.0
021_Loose_Sed_Molasse	2200.0
022_Loose_Sed_Po	2200.0
030_Con_Sed	2400.0
031_Con_Sed_Molasse	2400.0
032_Con_Sed_Po	2698.198993
04_U_Crust_Apennine	2720.0
05_U_Crust_Distant_Dense	2720.0
06_U_Crust_Moldanubia	2699.999998
07_U_Crust_Bohemia	2740.0
08_U_Crust_North_east	2679.999999
09_U_Crust_Saxothuringia	2700.0
10_U_Crust_Vosges	2659.999998
11_U_Crust_Molasse	2720.0
12_U_Crust_E_Alps	2739.999999
13_U_Crust_nae_Clue	2730.0
14_U_Crust_W_Alps	2700.0
15_U_Crust_Po	2700.0
16_U_Crust_NE_Adria	2629.999984
17_U_Crust_Ivrea	2700.0
18_U_Crust_SE_Adria	2699.999999
19_L_Crust_North_West	2761.379007
20_L_Crust_North	2917.336256
21_L_Crust_Europe	2789.616911
22_L_Crust_North_East	3106.348911
23_L_Crust_West	2960.0
24_L_Crust_E_Alps	2946.746194
25_L_Crust_East	3049.999995
26_L_Crust_Ivrea	3103.011971
27_L_Crust_Liguria_and_Apennine	2820.0

Name	Density[kg/m³]
031_Con_Sed_Molasse	2400.0
032_Con_Sed_Po	2698.198993
04_U_Crust_Apennine	2720.0
05_U_Crust_Distant_Dense	2720.0
06_U_Crust_Moldanubia	2699.999998
07_U_Crust_Bohemia	2740.0
08_U_Crust_North_east	2679.999999
09_U_Crust_Saxothuringia	2700.0
10_U_Crust_Vosges	2659.999998
11_U_Crust_Molasse	2720.0
12_U_Crust_E_Alps	2739.999999
13_U_Crust_nae_Clue	2730.0
14_U_Crust_W_Alps	2700.0
15_U_Crust_Po	2700.0
16_U_Crust_NE_Adria	2629.999984
17_U_Crust_Ivrea	2700.0
18_U_Crust_SE_Adria	2699.999999
19_L_Crust_North_West	2761.379007
20_L_Crust_North	2917.336256
21_L_Crust_Europe	2789.616911
22_L_Crust_North_East	3106.348911
23_L_Crust_West	2960.0
24_L_Crust_E_Alps	2946.746194
25_L_Crust_East	3049.999995
26_L_Crust_Ivrea	3103.011971
27_L_Crust_Liguria_and_Apennine	2820.0
28_L_Crust_Adria_and_Corsica	3032.036036
29_Mantle	3506.580529
30_Mantle_2	3406.657679
31_Base	3314.999991
Top	0.0
reference	0.0

(C)

FIGURE 8
The 3D density model. **(A)** The 3D model looking north-west. The Free air anomalies are outlined above the actual model. Below, the pink layer shows the location of vertical sections defining the 3D model and the locations of the model stations (pink dots) from which the model's Free air gravity was calculated. The seismic Moho (Grad et al., 2009) is shown in green at the western edge of the model. Below is a view of the model crust and upper mantle with different structures (various colors) down to a depth of 50 km. Below (dark brown) is the mantle voxel cube, part of the density model, containing velocities converted to densities (Kumar et al., 2022). **(B)** View of the central part of the 3D model between the French coast and the island of Corsica. In contrast to Figure 8A, this view omits the plane of the stations. The vertical structures and seismic profiles from Figure 4 are shown: Lisa01, MS47, P01, and P02+Makris (in yellow), along with an additional profile from Le Breton (personal communication). **(C)** Used model densities. Further explanations are in the text.

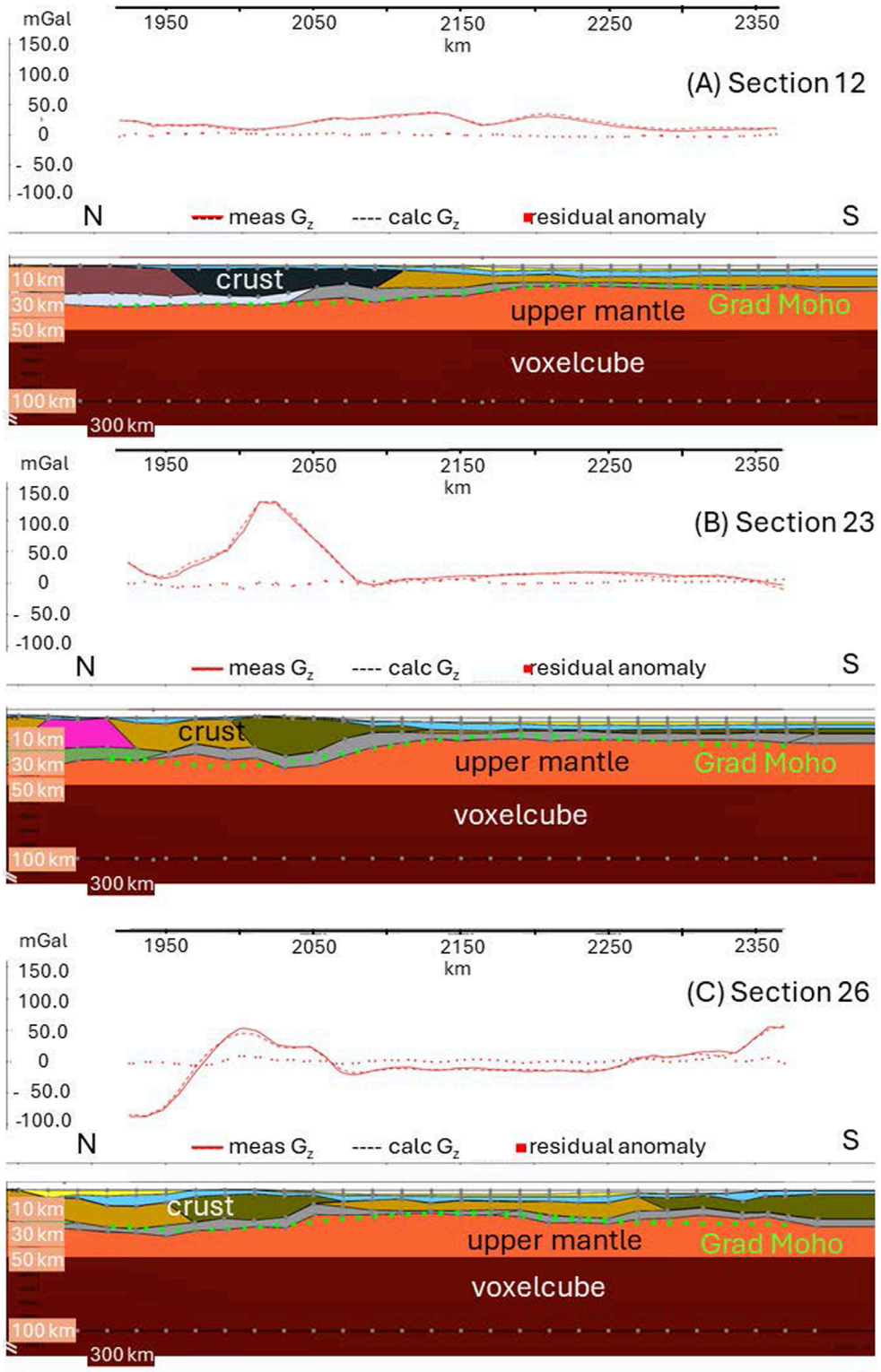

FIGURE 9
Three examples from the 31 vertical model sections of our density model. Each upper box shows the three gravity profiles: the solid curve is the reference gravity (Free air anomalies), the dashed curve is the model gravity, and the dotted curve is the residual; lower boxes show the vertical cross-section. **(A)** The westernmost cross-section 12 crosses a gravity high off the French coast. **(B)** Vertical cross-section 23 is positioned along the gravity high in the basin center. **(C)** Cross-section 26 runs along the north-south oriented eastern gravity minimum. The small green dotted line in each figure shows the course of the "European Moho" along the cross-sections. Units along the *y*-axis are km of UTM coordinates. Model densities and their colors correspond to densities in Figure 8C.

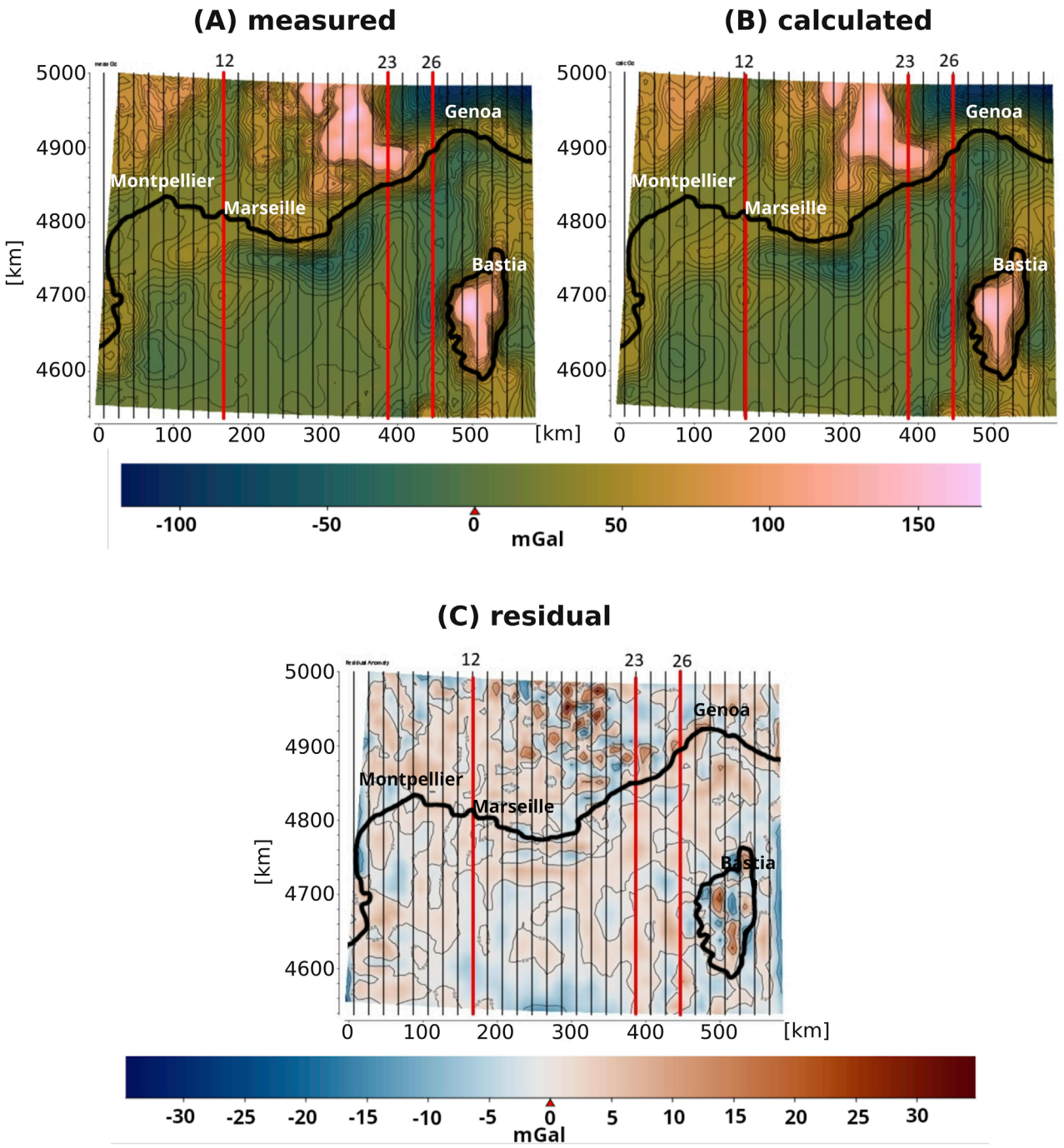

FIGURE 10
The resulting gravity maps of the Liguro-Provençal Basin are shown in the upper panel from left to right: **(A)** Free air anomaly, **(B)** calculated model gravity; lower panel **(C)** - residual field of both. The shortwave residuals are now clearly visible. These shortwave anomalies in the French-Italian Alps and Corsica regions are due to the locally very pronounced topography, which the model cannot capture accurately enough. However, these anomalies do not affect the overall result. The thick black contour line represents the zero line. Reddish lines correspond with the cross-sections shown in Figure 9.

representing a detached plate in the Alps and a connected plate in the northern Apennines, consistent with observed seismicity at intermediate depths, was adopted. It captures the study area's topography and vertical surface velocities, serving as a first approximation to a constrained upper mantle.

The gravity field caused by the density inhomogeneities in the upper mantle between 50 and 300 km depth is shown below in Figure 15. This figure shows that neglecting the gravity anomalies in the upper mantle significantly effects on the shape and magnitude of the gravity in the study area: it varies

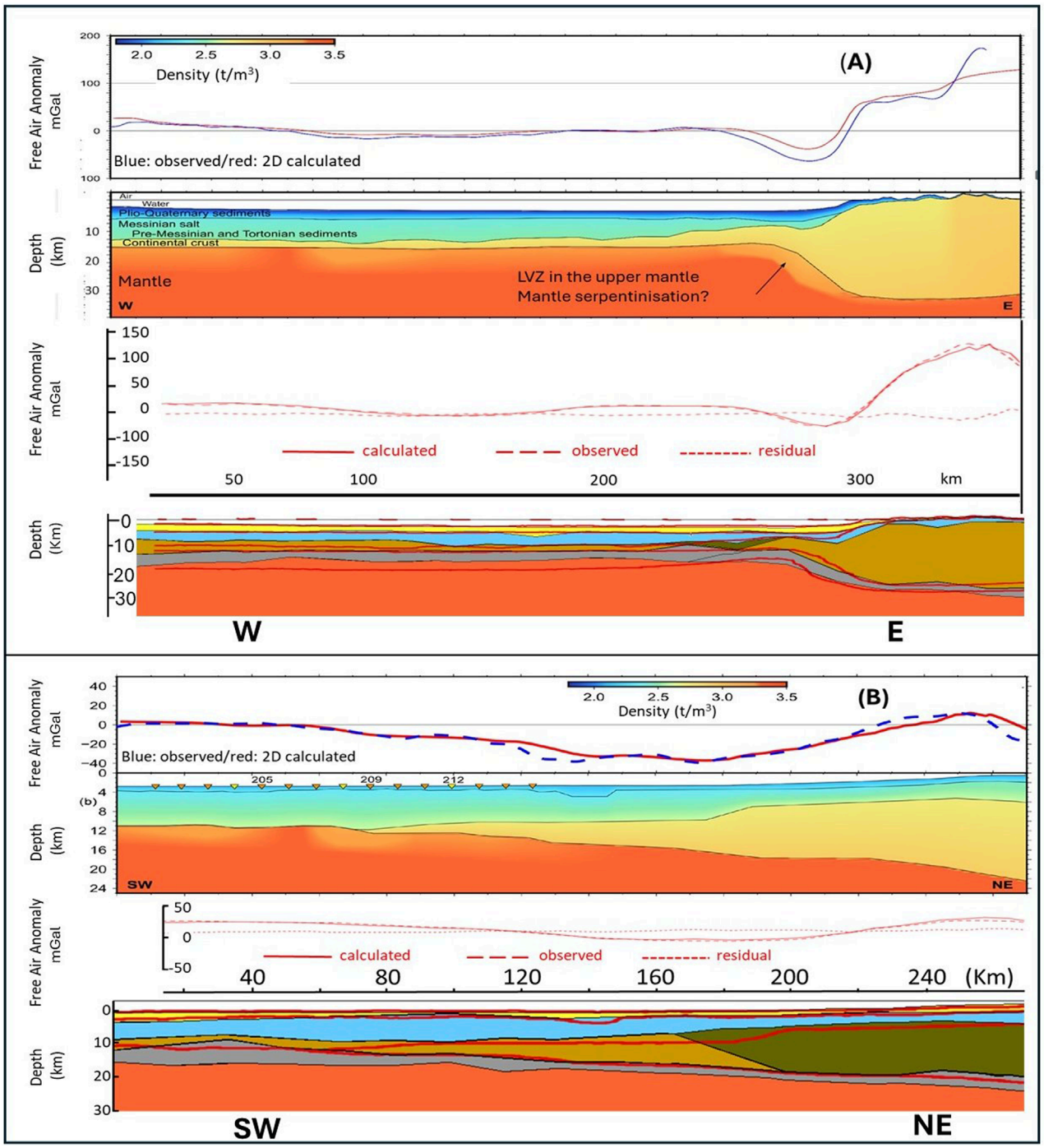

FIGURE 11
Comparison of the 2D gravity modeling based on refraction seismic data along profiles P01 and P02-Makris (LOBSTER, Dannowski et al. (2020)) with our 3D modeling results. The locations of the two profiles are shown in Figure 4. **(A)** The upper part presents the 2D modeling along the west-east oriented P01 profile, with Corsica on the right margin. The lower section of **(A)** displays our 3D modeling results for the P01 profile, showing an improved fit to the free-air anomaly. **(B)** Similarly, the upper part shows the 2D model from Dannowski et al. (2020), while the lower part shows our 3D modeling results for the P02+Makris profile. The 3D model densities are indicated, with red lines in the 3D sections marking the boundaries of bodies from the 2D models. The 3D model densities match those in Figure 8C.

from $-30 \times 10^{-5} m/s^2$ (−30 mGal) in the southwest to $70 \times 10^{-5} m/s^2$ (70 mGal, maximum) in the Apennines in the northeast.

In addition to the north-south profiles through the 3D model shown in Figures 9, 11 presents 3D model slices along arbitrary orientations—specifically along profiles P01 and P02-Makris (refer to Figure 4). This allows for a direct comparison between the 2D modeling by Dannowski et al. (2019) and our recent 3D modeling (Figures 11A,B), confirming overall agreement between the two.

Notably, the free-air gravity rise in the Corsica region (Figure 11A, southeast) is primarily driven by topographic elevation. The significant gravity low around profile km 290 in the 3D model is attributed to thicker sediment layers, consolidated sediments (depicted in yellow and blue), and the submersion of mantle structures (gray and orange). Both models reveal similar general structures and density distributions; however, the 3D model provides a better fit to the gravity field in specific areas, such as west of Corsica.

Figure 11B highlights a dipping Moho interface toward the Italian mainland. Both models accurately represent the crust-mantle transition zone in the Liguro-Provencal Basin. The low-velocity zone (LVZ) in the upper serpentinized mantle may also be interpreted as a high-velocity zone (HVZ), potentially indicating rift-related underplating in the crust. The modeling confirms higher average densities and elevated gravity values in the central Ligurian Basin. Velocity and density modeling results are consistent with the seismic findings of Dannowski et al. (2020), which report a 6–8 km thick sedimentary cover and a seismic Moho at depths of 11–15 km below the sea surface.

In summary, the new constrained 3D modeling shows a satisfactory fit between the Free air anomaly and the modeled Free air anomaly. Deviations in the residual gravity map are within $\pm 5 \times 10^{-5} m/s^2$ (±5 mGal) in Figure 10. The error we report for the modeled field is also ± 5 mGal. Larger deviations occur only in the southwestern Alps and Corsica, primarily due to the need for more vertical planes to approximate the topography/Free air anomaly in mountainous areas. However, adding more planes for extensive model areas, such as the entire offshore area, would unnecessarily complicate the model.

5.6 Gravitational potential energy (GPE)

Gravitational Potential Energy (GPE) is a key concept in geophysics, representing the energy stored in an object due to its position in the gravity field. It is directly proportional to the object's mass and its height relative to a reference point. The modeling software calculates the GPE at the gravity stations' positions, resulting in a 1D calculation. The 2D distribution shown in the maps in Figure 12 is derived through interpolation.

Background: 1) Dependence on Mass: GPE is directly proportional to an object's mass. Heavier objects have more GPE at the same height. 2) Dependence on Altitude: GPE is directly proportional to the height above a reference point. Higher elevations result in greater GPE. 3) Gravitational Field Strength: On Earth, g is approximately 9.81 m/s^2 but varies with location and altitude. 4) Tectonic Reference Level (TRL): The choice of reference level is crucial for GPE calculations and vertical stress. Following Coblentz et al. (1994), we assume an average value of 2.373 × 1,014 N/m, equivalent to the potential energy of continental plates and basins with topography below sea level.

GPE helps explain various geophysical phenomena. Applying current processing methods to our gravity data set provides valuable insights, as demonstrated in previous studies (e.g., Ghosh et al., 2009; Flesch and Kreemer, 2010; Schmalholz et al., 2014; Neres et al., 2018).

The GPE per unit area (A) is defined as:

$GPE = mgh/A$, given $m = \rho hA$ we get:

$GPE = \rho gh^2$

where m is mass, g is gravity, h is height, and ρ is rock density. For inhomogeneous density columns, we use piecewise constant densities:

$GPE = g\sum \rho_i h_i$

The unit of GPE is kg/s^2 ($Joule/m^2$ or N/m). Comparing GPE with stress, we see:

$GPE = \sum \sigma_i h_i$

where σ_i is the stress contribution of layer i with constant density ρ_i and thickness h_i. In a constant density environment, stress increases linearly with depth, while GPE increases quadratically.

The Ligurian Sea's stress regime results from the convergence of the African and European plates. This collision shapes the region's tectonics. Additional factors influencing the Ligurian margin include the rollback of the Ionian-Adriatic subduction, gravitational collapse of the Apenninic lithosphere, and lateral extrusion of the southwestern Alps (Morelli et al., 2022). Due to this complexity Eva and Solarino (1998) suggested that the Ligurian Basin should be analyzed separately from the adjacent Alpine chain. Compression within the Ligurian Sea may reactivate fault systems in the Nice Arc. The GPE distribution in the Liguro-Provençal Basin reveals a complex interplay of tectonic forces. Positive GPE values in the central region and around Corsica indicate thicker or denser crust and this stored energy translates into compressional forces as the crust attempts to reach gravitational equilibrium. Lower GPE near the French coast suggests thinner or less dense crust. These areas are often associated with compressional forces rather than extensional forces, as the crust is under less gravitational potential energy stress. This complex stress environment results from the Ligurian Basin's opening or extension, influenced by broader plate interactions. The coexistence of these varying GPE values highlights the dynamic interplay of tectonic forces in the region, which is corroborated by independent studies that describe similar heterogeneous stress distributions and their effects on geological structures (e.g., Baroux et al., 2001).

5.7 Euler deconvolution

Euler Deconvolution (ED) is a mathematical method used in geophysics to estimate the depths and locations of underground sources in potential fields (Reid et al., 1990; Pašteka, 2006; Saleh and Pašteka, 2012). ED analyzes gradients or derivatives of observed potential field data to infer subsurface sources, which are modeled as simple geometric bodies (spheres, cylinders). ED provides estimates for:

- Depth (Z) of the source below the Earth's surface.
- Location coordinates (X, Y) of the source.

ED assumes simplified source shapes and may not always represent complex geological structures accurately. It is often used with other geophysical and geological data to refine interpretations and improve subsurface exploration accuracy. In our analysis, ED is applied to both Bouguer and Free air gravity using the REGDER software (Pašteka, pers. comm).

The main parameters for the Euler Deconvolution (ED) are specified above the Figure A1 in the supplementary materials: for the Bouguer anomaly analysis, a window size (WS) of 7 units is used, and for the Free air anomaly (FA), the WS is 5 units. The structure

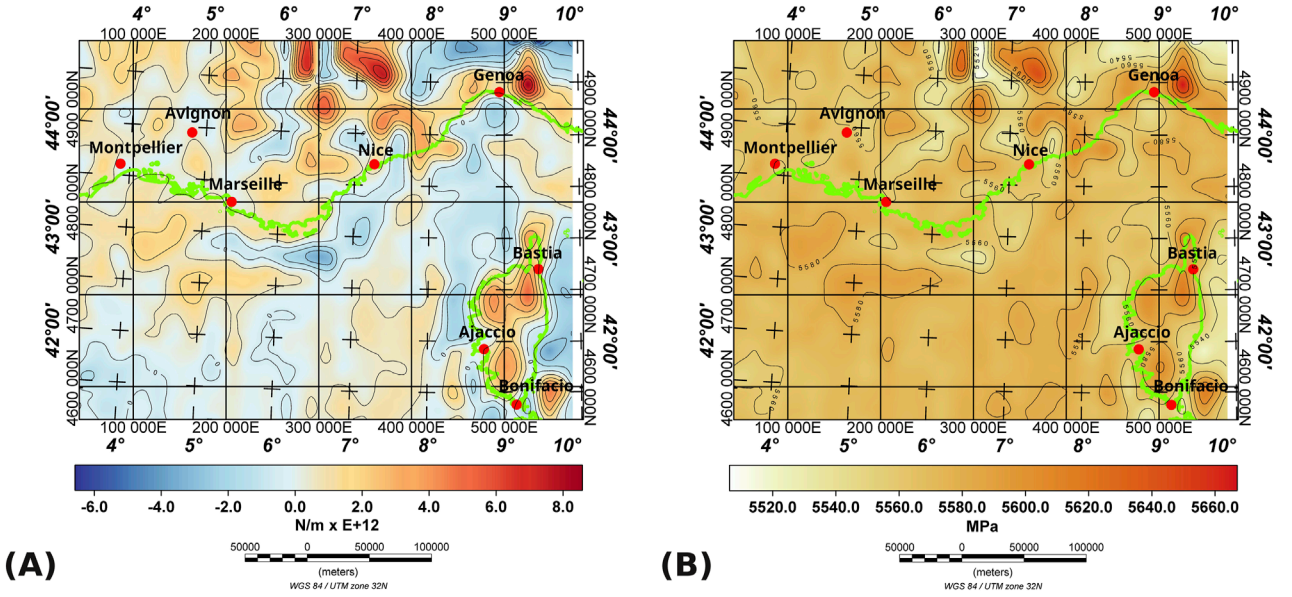

FIGURE 12
The relationship between gravitational potential energy (GPE) and vertical stress in the Earth's crust is closely interconnected, as GPE directly impacts the forces within the crust. **(A)** Regions with high GPE, such as thick sedimentary basins, have greater mass above a given depth (TRL). This increased mass results in higher vertical stress due to the greater weight of the overlying layers. **(B)** Vertical stress (ZZ) distribution in the Ligurian basin is based on the density model. Regions with higher GPE produce higher vertical stress, leading to geological processes such as compression, densification, and potential deformation of the Earth's crust.

index is set to 2 for both fields, indicating a three-dimensional borehole. In the Liguro-Provençal Basin, the analyses differ for the two fields. For the Bouguer Anomaly (BA), only a few source points are identified in the Ligurian Sea, with most sources located around Corsica and the southwestern Alpine arc. The concentration of source points in the southern area aligns with the anomaly in the shape curvature (Figure 6). The FA analysis also shows a concentration of Euler source points, though strong gradients in the Free air anomaly elsewhere limit its utility. Regarding the question of whether the gravity field indicates a possible rift structure, the ED results alone do not provide a conclusive answer. Detailed ED results are provided in the Appendix.

6 Interpretation and discussion

Interpreting static gravity fields is inherently ambiguous due to theoretical limitations, and independent constraints are essential to reduce this ambiguity. In previous sections, we introduced independent data (seismic, seismology, geology) and relevant literature. Here, we compare the results of gravity field processing with these independent sources to address our key questions from the introduction (Section 1).

6.1 Crustal architecture and tectonic evolution

Rollet et al. (2002) discussed back-arc extension, tectonic inheritance, and volcanic activity in the Ligurian Sea, identifying three crustal domains: 1) continental thinned margins, 2) transition areas to the basin, and 3) a narrower atypical oceanic area. Margin structures feature tilted blocks forming syn-rift sedimentation and segmentation. Using Rollet et al.'s (2002) nomenclature, the terraced Bouguer anomaly (Figure 13B) shows: "orange" colors represent "margins," dark pink/reddish colors indicate the "transitional domain," and lighter pink areas in the central part represent "atypical oceanic crust." Structurally, this area is at a relatively high bathymetric position in the 3D model (Figure 9). This fit is expected as Rollet et al. (2002) also based their interpretation on gravimetric and magnetic data.

With the results of Canva et al. (2021) we identify a correlation between areas of possibly exhumed mantle and the central positive anomaly in the Free air gravity anomaly. According to their interpretation, the bright pink stripe in the Bouguer anomaly (Figure 13B) could also represent areas of exhumed mantle. This correlation is supported by travel time tomography results from the SEFASILS cruise (Canva et al., 2021) and the southeastern part of the P02-Makris profile (Dannowski et al., 2020). In the neighboring Tyrrhenian Sea, seismic studies reveal exhumed mantle that is linked to the opening of the basin (Prada et al., 2016). There, the authors could constrain in space and time that processes of mantle exhumation, and later magmatic intrusions of MOR-type and intraplate basaltic rocks were involved in the opening of the basin. Consistent with Rollet et al. (2002), we interpret the darker pink area in the Bouguer anomaly as hyper-extended crust formed during the rifting phase.

6.2 Moho depth and crustal thickness

In areas with continental thinned margins, the Moho depth is around 20–25 km due to significant crustal thinning from extensional tectonics. Transitional zones between continental

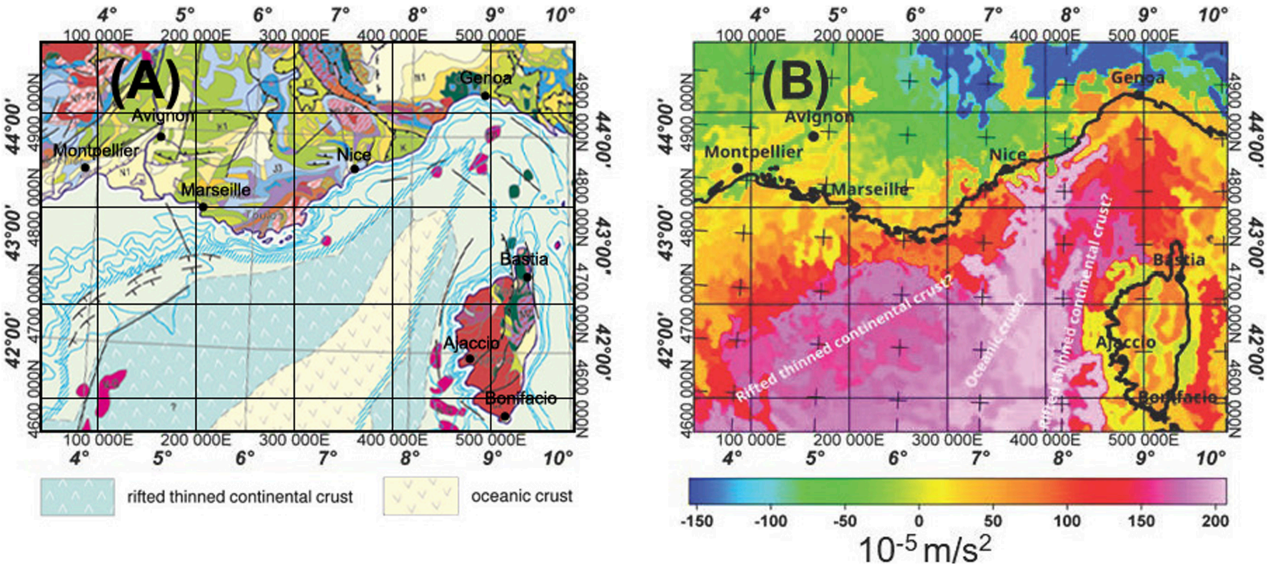

FIGURE 13
Comparing the geological map in **(A)** (Asch, 2005) with the terraced Bouguer anomaly **(B)** reveals similarities in the three domains identified by the author: "rifted thinned continental crust," "oceanic crust," and "rifted thinned continental crust." Darker and lighter purple areas in the Bouguer anomaly correlate with these geological features.

margins and oceanic crust typically exhibit Moho depths of 15–20 km. In the narrower atypical oceanic areas, the Moho is shallower, around 10–15 km, indicating more significant crustal thinning and extension compared to continental margins. Overall, the Moho depth in the Ligurian basin ranges from 10 to 25 km, varying with the specific tectonic and geological context of each sub-region.

6.3 Rifting and continental break-up

In the late 1970s, Giese et al. (1978) provided early insights into the complex offshore conditions of the Ligurian Sea, Western Alps, and Apennines. In "Alps, Apennines, Hellenides" (Closs et al., 1978), they noted the static and dynamic interdependencies of the Adriatic microplate with the Western Alps and the Apennine Arc, assuming an oceanic crust with a mantle depth of 15 km in the Ligurian Sea. Our 3D modeling (Section 5.3.1) shows a Moho depth of about 12–16 km in the central Ligurian Sea. These results, combined with structural comparisons (Figure 14), indicate that the Ligurian Sea's opening and boundary structures are controlled by the interplay between inherited crustal heterogeneity and external tectonic forces, such as subducting lithosphere rollback.

According to Rollet et al. (2002), various crustal domains can be identified, which are also reflected in our interpretation of gravity field data. The first domain, demarcated by a reddish-pink line and labeled "TD," corresponds to the transitional domain. The white line, labeled "AOD," delineates the extent of the (inner) "atypical oceanic domain," characterized by an elevated Moho position and a central gravity high in both the free-air and Bouguer anomalies (Figure 3). The bright yellow line in the center, labeled "ODG," represents the "oceanic domain" as defined by Gueguen et al. (1998), marked by the central maximum in the gravity field. Light and dark blue lines, based on the interpretation of Asch (2005) and previously illustrated in Figure 13A, differentiate between oceanic crust in the center and a "rifted, thinned continental crust." The latter is distinguished by lower free-air anomaly gravity values and significantly deeper Moho levels compared to the central high. Additionally, a red dashed line off the west coast of Corsica in the east indicates a proposed fracture zone, characterized by a steep gradient in the gravity field. No significant differences were found between our results and those from the referenced studies.

Dessa et al. (2020) characterized the northern Ligurian Sea as a geologically complex offshore region, influenced by multiple phases of tectonic deformation. They emphasized the role of salt structures, particularly along a narrow zone approximately between coordinates 43°20′N/8°00′E and 43°50′N/8°30′E, as well as deeper crustal tectonics, in controlling sedimentation patterns. Due to the regional scale of our 3D model, these localized features are too small to be resolved at high spatial resolution. Nonetheless, a local minimum in the free-air gravity anomaly (Figure 3C) and the interpretation of gravitational potential energy (GPE) in conjunction with the vertical stress map (Figure 12) may indicate morphological effects and accumulation of salt deposit accumulation within the crust.

Morelli et al. (2022) provided a detailed reconstruction of the morpho-structural setting and tectonic evolution of the Alpine and Apennine margins and the Ligurian Sea. Their analysis of bathymetric and geophysical data reveals a close relationship between recent active tectonics and the morpho-dynamic evolution of the Ligurian basin margin. This relationship is particularly evident in the Alpine margin, where uplift and inherited structures under compressive regimes are associated with widespread seismicity, showing spatial correlations with the GPE and stress maps in Figure 12. Figure 15 presents a map of the voxel cube gravity

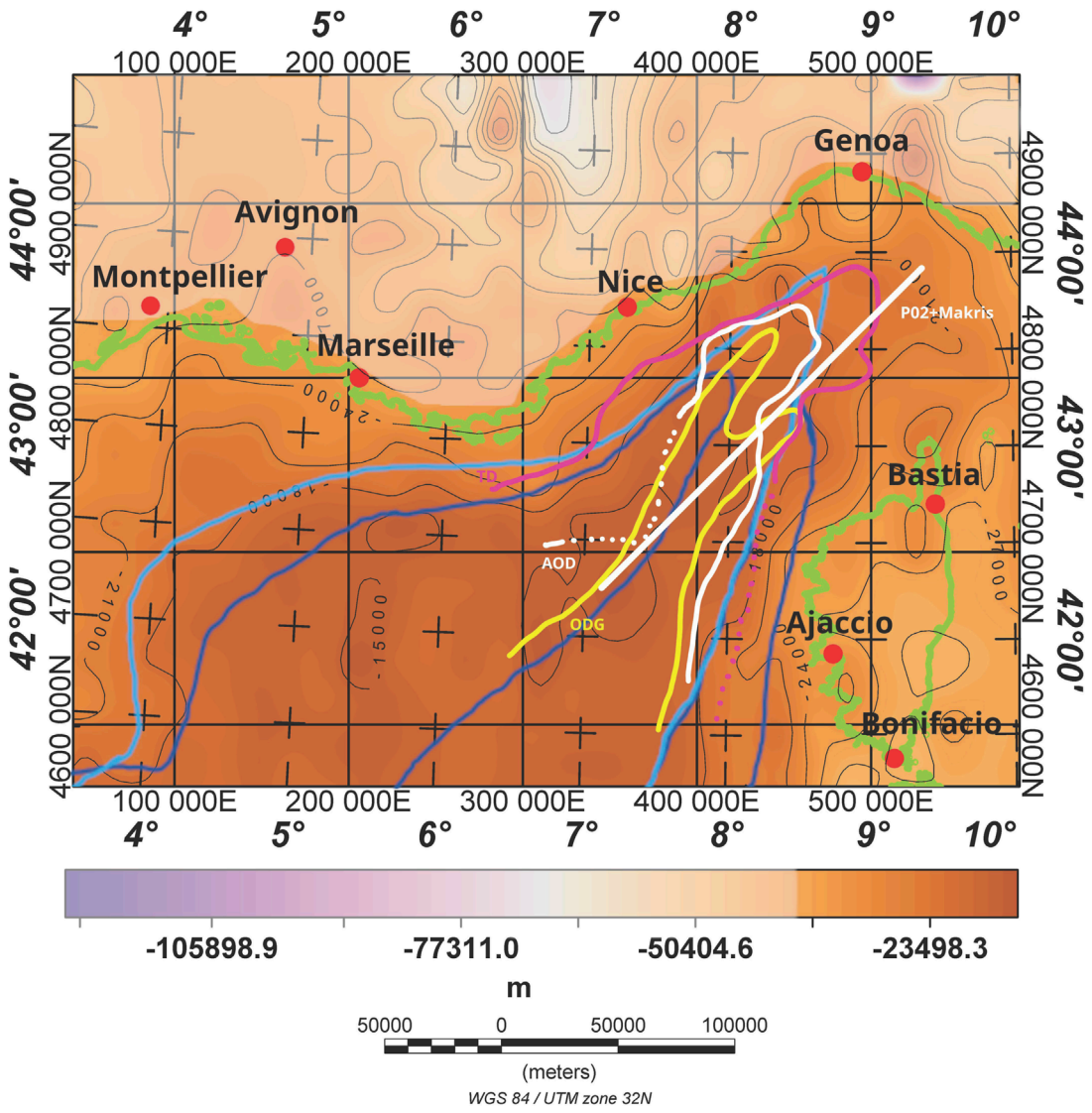

FIGURE 14
The overlay of proposed crustal domain boundaries from Asch (2005) (light and dark blue), Rollet et al. (2002) (reddish-pink and white lines), and Gueguen et al. (1998) (bright yellow line) after Dannowski et al. (2020) on the model Moho map shows good alignment with the main contours of the Moho and the central Bouguer gravity high (Figures 13B, 3A). For more information, refer to the text. The straight white line in the center indicates the position of the P02+Makris seismic profile from Figure 4.

effect superimposed on earthquake distribution, indicating an accumulation of earthquakes in areas with higher gravity field gradients. The voxel cube contains densities converted from velocities at depths between 50 and 300 km, highlighting the notable coincidence of hypocenters and gravity field shapes.

Our investigations reveal highly segmented gravity fields in the Liguro-Provençal Basin, as evidenced by the residual Bouguer gravity (Figure 3B), Free air anomaly (Figure 3C), shape curvature (Figure 6), and clustering of the terraced gravity fields (Figures 7, 13B). This level of resolution was previously unattainable. However, it remains uncertain whether these anomalies are definitively part of a rift structure. Comparisons with other regions, such as the South China Sea (e.g., Hagen, 2021), show much clearer gravity signals associated with rift structures. Seismic data from the LOBSTER experiment and structural evidence from the sefasils experiment suggest the deep reflection horizon in the south corresponds to the Moho, while shallower reflections in the north are attributed to the base of the sediment (Canva et al., 2021). The extensive salt complex observed may account for the narrow minimum in our residual gravity maps in the central Liguro-Provençal Basin. However, these local structures were not the primary focus of our 3D modeling due to the required resolution.

From the perspective of gravity field analysis (Bouguer, Free air anomaly, and residual fields), terracing and clustering, curvature, GPS, and 3D modeling indicate that rifting has likely influenced the basin's geological evolution. To summarize these findings, we provide a hierarchical processing approach that could be beneficial for similar studies in other regions:

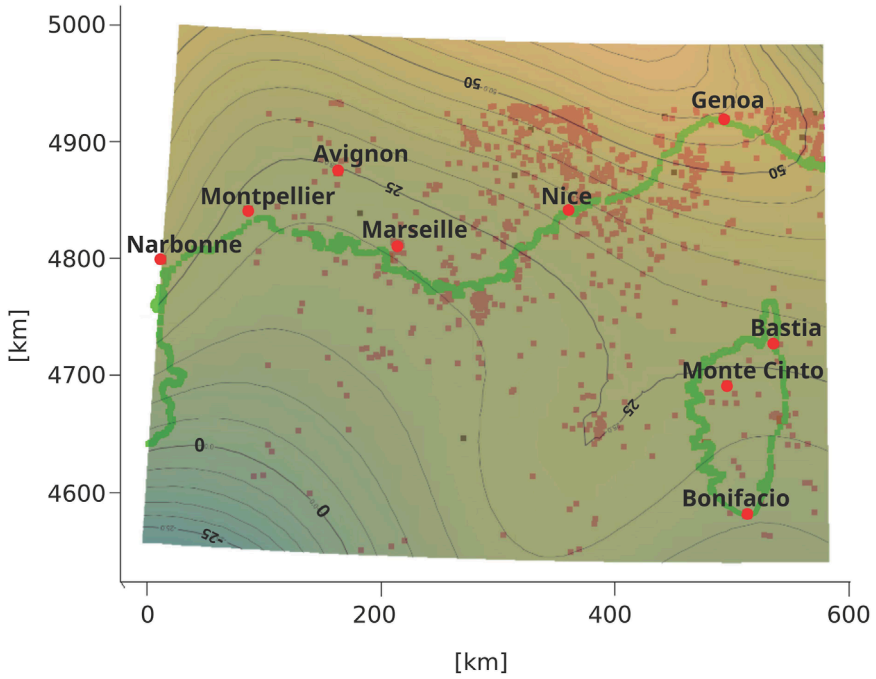

FIGURE 15
The voxel cube gravity effect (in 10^{-5} m/s^2) and earthquake locations (epicenters with focal depths ≤ 50 km) indicate that most earthquakes occur in areas with strong gravity field gradients. These gradients correspond to lithospheric and upper mantle density differences that could induce stress. This is particularly noticeable at the isoline tip in the central part of the Ligurian Sea, west of Corsica.

- AAGRG and smoothed Free air anomaly (chapter 3.3) ⇒ strong indication
- Shape curvature (chapter 5.1) ⇒ strong indication
- Terracing and clustering results (chapter 5.2) ⇒ strong indication
- Combined interpretation (chapter 6) ⇒ strong indication
- 3D-modeling (chapter 5.3) ⇒ moderate indication
- Gravitational potential energy (chapter 5.4) ⇒ moderate indication

7 Conclusion

The Liguro-Provençal Basin, located in the northwestern Mediterranean Sea, forms part of the broader Western Mediterranean Basin and has been shaped by the convergence of the African and Eurasian tectonic plates. This convergence has given rise to a variety of geological structures, including subduction zones, thrust faults, and basins. Unlike classical continental rifts, such as the East African or Rio Grande Rifts, the Liguro-Provencal Basin is a complex geological feature shaped by multiple tectonic processes. While it exhibits some extensional characteristics, it does not fit the typical profile of a continental rift. Instead, the basin has experienced both compressional and extensional forces due to the complex tectonic interactions within the Mediterranean region. This combination of forces has led to the development of sedimentary basins, including the Liguro-Provençal Basin, whose geological evolution is far more intricate than a simple rift system.

A key outcome of our 3D modeling and gravity field analysis is the confirmation of a Moho depth of approximately 12–16 km in the central Ligurian Sea, which aligns with the findings of previous seismic studies that reached similar conclusions without incorporating gravity field data. The integration of gravitational potential energy (GPE) and vertical stress analyses has proven extremely valuable, offering insights into the distribution of forces related to the gravity field. These force distributions provide a framework for linking gravity field analysis with geodynamic interpretations, which often differ from interpretations of static fields like gravity.

Our intensive gravity field analysis, as demonstrated here, serves as a powerful tool for spatially mapping rifted areas, complementing seismic or drilling data, which typically offer information along limited transects. Overall, the Moho depth in our 3D model of the Ligurian Basin varies between 15 and 25 km, reflecting differences in the tectonic and geological settings of various sub-regions.

Data availability statement

The structural data and related IGMAS+ model will be shared on reasonable request to the corresponding author. The Alpine gravity database 2020 with Bouguer and Free air anomalies is available from GFZ Data Services (Zahorec et al., 2020).

Author contributions

H-JG: Conceptualization, Data curation, Formal Analysis, Funding acquisition, Investigation, Methodology, Project administration, Resources, Software, Supervision, Validation, Visualization, Writing–original draft, Writing–review and editing. RS: Conceptualization, Data curation, Investigation, Methodology, Software, Visualization, Writing–review and editing. AD: Conceptualization, Data curation, Investigation, Methodology, Project administration, Validation, Visualization, Writing–review and editing. DA: Conceptualization, Data curation, Formal Analysis, Software, Validation, Visualization, Writing–review and editing. AK: Conceptualization, Formal Analysis, Investigation, Methodology, Software, Writing–review and editing. MS-W: Conceptualization, Formal Analysis, Funding acquisition, Investigation, Methodology, Project administration, Resources, Supervision, Validation, Writing–review and editing.

Funding

The author(s) declare that financial support was received for the research, authorship, and/or publication of this article. The studies were funded by the German Research Foundation (DFG) under the contracts GO380/36-1, SCHE 674/7-1 and SCHE 674/8-1 in the framework of the SPP 2017.

Acknowledgments

The authors gratefully acknowledge funding from the Deutsche Forschungsgemeinschaft (DFG) for the project "Deformation Patterns in Relation to the Deep Configuration of the Lithosphere of the Alps and Their Forelands (DEFORM)" within the Special Priority Program 2017. We extend our sincere thanks to our colleagues in the AlpArray Gravity Research Group (AAGRG), the Special Priority Program 2017 (Mountain Building in Four Dimensions, MB4D), and the IGMAS+ team for their excellent collaboration. We are particularly indebted to Dr. Sabine Schmidt and Christian Plonka for their continuous support in resolving software issues, Dr. Cameron Spooner for compiling the 3D density Alpine model, and Dr. Judith Bott for her ongoing interest and valuable insights regarding density modeling. We would like to thank Dr. Kristine Asch (BGR, Hannover, Germany) for permission to use sections of her Geological Map of Europe at a scale of 1:5 million.

Conflict of interest

All authors declare that the research was conducted in the absence of any commercial or financial relationships that could be construed as a potential conflict of interest.

Publisher's note

All claims expressed in this article are solely those of the authors and do not necessarily represent those of their affiliated organizations, or those of the publisher, the editors and the reviewers. Any product that may be evaluated in this article, or claim that may be made by its manufacturer, is not guaranteed or endorsed by the publisher.

Supplementary material

The Supplementary Material for this article can be found online at: https://www.frontiersin.org/articles/10.3389/feart.2024.1475025/full#supplementary-material

References

Alvers, M. R., Barrio-Alvers, L., Bodor, C., Götze, H.-J., Lahmeyer, B., Plonka, C., et al. (2015). *Quo vadis* inversión? *First Break* 33. doi:10.3997/1365-2397.33.4.79746

Alvers, M. R., Götze, H.-J., Anikiev, D., and Plonka, C. (2023). Inversion of potential fields by interactive optimization of 3d subsurface models using a spring-based space warping and evolution strategy. *GEOPHYSICS* 88, G79–G93. doi:10.1190/geo2022-0222.1

Anikiev, D., Götze, H.-J., Bott, J., Gómez-García, A. M., Gomez Dacal, M. L., Meeßen, C., et al. (2021). "Interdisciplinary data-constrained 3-d potential field modelling with igmas+," in *EGU general assembly conference abstracts* (Göttingen, Germany: Copernicus GmbH). EGU21–2964. doi:10.5194/egusphere-egu21-2964

Anikiev, D., Götze, H.-J., Plonka, C., Scheck-Wenderoth, M., and Schmidt, S. (2023a). Igmas+: interactive gravity and magnetic application system doi:10.5880/GFZ.4.5.IGMAS

Anikiev, D., Götze, H.-J., Plonka, C., Schmidt, S., Bott, J., and Scheck-Wenderoth, M. (2023b). Interactive optimisation of 3-D subsurface models using potential fields. *Tech. Rep*. doi:10.5194/egusphere-egu23-1860

Asch, K. (2005). *IGME 5000: 1 : 5 Million International Geological Map of Europe and Adjacent Areas - final version for the internet*. Hannover: BGR.

Baroux, E., Béthoux, N., and Bellier, O. (2001). Analyses of the stress field in southeastern France from earthquake focal mechanisms. *Geophys. J. Int.* 145, 336–348. doi:10.1046/j.1365-246x.2001.01362.x

Barruol, G., Deschamps, A., and Coutant, O. (2004). Mapping upper mantle anisotropy beneath se France by sks splitting indicates neogene asthenospheric flow induced by apenninic slab roll-back and deflected by the deep alpine roots. *Tectonophysics* 394, 125–138. doi:10.1016/j.tecto.2004.08.002

Canva, A., Dessa, J.-X., Ribodetti, A., Beslier, M.-O., Schenini, L., Larroque, C., et al. (2021). Structural inversion of the north Ligurian margin: results from the sefasils experiment doi:10.5194/egusphere-egu21-9759

Closs, H., Roeder, D., and Schmidt, K. (eds.) (1978). Alps, Apennines Hellenides geodynamic investigation along geotraverses by an international group of geoscientists, vol. report 38 of *Scientific report/inter-union commission on geodynamics* (Stuttgart, Germany: Schweizerbart'sche Verlagsbuchhandlung). ISBN: 978-35-106-5083-5).

Coblentz, D. D., Richardson, R. M., and Sandiford, M. (1994). On the gravitational potential of the earth's lithosphere. *Tectonics* 13, 929–945. doi:10.1029/94tc01033

Contrucci, I., Nercessian, A., Béthoux, N., Mauffret, A., and Pascal, G. (2001). A Ligurian (western mediterranean sea) geophysical transect revisited. *Geophys. J. Int.* 146, 74–97. doi:10.1046/j.0956-540x.2001.01418.x

Cooper, G. R. J. (2020). An improved terracing algorithm for potential-field data. *GEOPHYSICS* 85, G109–G113. doi:10.1190/geo2019-0129.1

Dannowski, A., Kopp, H., Grevemeyer, I., Lange, D., Thorwart, M., Bialas, J., et al. (2020). Seismic evidence for failed rifting in the Ligurian basin, western alpine domain. *Solid earth.* 11, 873–887. doi:10.5194/se-11-873-2020

Dannowski, A., Kopp, H., Grevemeyer, I., Lange, D., Thowart, M., Bialas, J., et al. (2019). Seismic evidence for failed rifting in the Ligurian Basin, western alpine domain. *Solid earth.* 11, 873–887. doi:10.5194/se-11-873-2020se-2019-187

Dessa, J.-X., Beslier, M.-O., Schenini, L., Chamot-Rooke, N., Corradi, N., Delescluse, M., et al. (2020). Seismic exploration of the deep structure and seismogenic faults in the Ligurian sea by joint multi channel and ocean bottom seismic acquisitions: preliminary results of the sefasils cruise. *Geosciences* 10, 108. doi:10.3390/geosciences10030108

Dessa, J.-X., Simon, S., Lelievre, M., Beslier, M.-O., Deschamps, A., Bethoux, N., et al. (2011). The grosmarin experiment: three dimensional crustal structure of the north Ligurian margin from refraction tomography and preliminary analysis of microseismic measurements. *Bull. la Société Géologique Fr.* 182, 305–321. doi:10.2113/gssgfbull.182.4.305

De Voogd, B., Nicolich, R., Olivet, J. L., Fanucci, F., Burrus, J., Mauffret, A., et al. (1991). First deep seismic reflection transect from the gulf of lions to sardinia (Ecorr-Crop profiles in western mediterranean). *Am. Geophys. Union (AGU)*, 265–274. doi:10.1029/GD022p0265

Doglioni, C., Harabaglia, P., Merlini, S., Mongelli, F., Peccerillo, A., and Piromallo, C. (1999). Orogens and slabs vs. their direction of subduction. *Earth-Science Rev.* 45, 167–208. doi:10.1016/S0012-8252(98)00045-2

Ebbing, J., Haas, P., Ferraccioli, F., Pappa, F., Szwillus, W., and Bouman, J. (2018). Earth tectonics as seen by GOCE—Enhanced satellite gravity gradient imaging. *Scientific Reports* 8 (1). doi:10.1038/s41598-018-34733-9

Eva, E., and Solarino, S. (1998). Variations of stress directions in the western alpine arc. *Geophys. J. Int.* 135, 438–448. doi:10.1046/j.1365-246x.1998.00649.x

Finetti, I., and Morelli, C. (1973). Geophysical exploration of the mediterranean sea. *Boll. Geofis. Teor. Appl.* 15, 263–340.

Flesch, L. M., and Kreemer, C. (2010). Gravitational potential energy and regional stress and strain rate fields for continental plateaus: examples from the central andes and Colorado plateau. *Tectonophysics* 482, 182–192. doi:10.1016/j.tecto.2009.07.014

Florio, G., and Lo Re, D. (2018). Terracing of potential fields by clustering methods. *Geophysics* 83 (4), G47–G58. doi:10.1190/geo2017-0140.1

Gailler, A., Klingelhoefer, F., Olivet, J.-L., Aslanian, D., and Technical, O. (2009). Crustal structure of a young margin pair: new results across the ligure–provencal basin from wide-angle seismic tomography. *Earth Planet. Sci. Lett.* 286, 333–345. doi:10.1016/j.epsl.2009.07.001

Gattacceca, J., Deino, A., Rizzo, R., Jones, D., Henry, B., Beaudoin, B., et al. (2007). Miocene rotation of sardinia: new paleomagnetic and geochronological constraints and geodynamic implications. *Earth Planet. Sci. Lett.* 258, 359–377. doi:10.1016/j.epsl.2007.02.003

Ghosh, A., Holt, W. E., and Flesch, L. M. (2009). Contribution of gravitational potential energy differences to the global stress field. *Geophys. J. Int.* 179, 787–812. doi:10.1111/j.1365-246x.2009.04326.x

Giese, P., Morelli, C., and Nicolich, R. (1978). "Review of the crustal structures of the northern apennines, the Ligurian sea and corsica," in *Alps, Apennines, Hellenides. Geodynamic Investigations along Geotraverses by an International Group of Geoscientists*. Editors H. Closs, D. Roeder, and K. Schmidt (Schweizerbart'sche Verlagsbuchhandlung), vol. report 38 of Scientific report/Inter-Union Commission on Geodynamics). ISBN: 978-35-106-5083-5.

Ginzburg, A., Makris, J., and Nicolich, R. (1986). European geotraverse: a seismic refraction profile across the Ligurian sea. *Tectonophysics* 126, 85–97. doi:10.1016/0040-1951(86)90221-0

Götze, H.-J., Anikiev, D., Sabine, S., Plonka, C., Scheck-Wenderoth, M., and Bott, J. (2023). "Is forward modeling still up to date? reflections on the 40 years of modeling gravity and magnetic fields," in *XXVIII General Assembly of the International Union of Geodesy and Geophysics (IUGG) (Berlin)* (Potsdam, Germany: GFZ German Research Centre for Geosciences). doi:10.57757/IUGG23-0291

Götze, H.-J., and Lahmeyer, B. (1988). Application of three-dimensional interactive modeling in gravity and magnetics. *GEOPHYSICS* 53, 1096–1108. doi:10.1190/1.1442546

Grad, M., Tiira, T., and Group, E. W. (2009). The mho depth map of the european plate. *Geophys. J. Int.* 176, 279–292. doi:10.1111/j.1365-246X.2008.03919.x

Gueguen, E., Doglioni, C., and Fernandez, M. (1998). On the post-25 ma geodynamic evolution of the western mediterranean. *Tectonophysics* 298, 259–269. doi:10.1016/s0040-1951(98)00189-9

Guerin, G., Rivet, D., Deschamps, A., Larroque, C., Mordret, A., Dessa, J., et al. (2019). High resolution ambient noise tomography of the Southwestern Alps and the Ligurian margin. *Geophysical Journal International* 220 (2), 806–820. doi:10.1093/gji/ggz477

Hagen, A. (2021). *A study of the thermal and petrophysical properties of a rift propagator*. Master's thesis. Kiel, Germany: Universität zu Kiel.

Handy, M. R., Ustaszewski, K., and Kissling, E. (2014). Reconstructing the alps–Carpathians–Dinarides as a key to understanding switches in subduction polarity, slab gaps and surface motion. *Int. J. Earth Sci.* 104, 1–26. doi:10.1007/s00531-014-1060-3

Hetényi, G., Molinari, I., Clinton, J., Bokelmann, G., Bondár, I., Crawford, W. C., et al. (2018). The alparray seismic network: a large-scale european experiment to image the alpine orogen. *Surv. Geophys.* 39, 1009–1033. doi:10.1007/s10712-018-9472-4

Jolivet, L., and Faccenna, C. (2000). Mediterranean extension and the africa-eurasia collision. *Tectonics* 19, 1095–1106. doi:10.1029/2000TC900018

Jolivet, L., Gorini, C., Smit, J., and Leroy, S. (2015). Continental breakup and the dynamics of rifting in back-arc basins: the gulf of lion margin: backarc rift and lower crust extraction. *Tectonics* 34, 662–679. doi:10.1002/2014tc003570

Jolivet, L., Romagny, A., Gorini, C., Maillard, A., Thinon, I., Couëffé, R., et al. (2020). Fast dismantling of a mountain belt by mantle flow: late-orogenic evolution of pyrenees and ligure-provençal rifting. *Tectonophysics* 776, 228312–312. doi:10.1016/j.tecto.2019.228312

Kodinariya, T. M., and Makwana, P. R. (2013). Review on determining number of Cluster in K-Means Clustering. *International Journal* 1 (6), 90–95.

Kopp, H., Lange, D., Dannowski, A., Thorwart, M., and Grevemeyer, I. (2023). Ligurian ocean bottom seismology and tectonics research (lobster). *Freie Univ. Berl.* doi:10.17169/REFUBIUM-41050

Kumar, A., Cacace, M., Scheck-Wenderoth, M., Götze, H.-J., and Kaus, B. J. P. (2022). Present-day upper-mantle architecture of the alps: insights from data-driven dynamic modeling. *Geophys. Res. Lett.* 49, e2022GL099476. doi:10.1029/2022gl099476

Le Breton, E., Brune, S., Ustaszewski, K., Zahirovic, S., Seton, M., and Müller, R. D. (2021). Kinematics and extent of the piedmont–Liguria basin – implications for subduction processes in the alps. *Solid earth.* 12, 885–913. doi:10.5194/se-12-885-2021

Le Breton, E., Handy, M. R., Molli, G., and Ustaszewski, K. (2017). Post-20 ma motion of the adriatic plate: new constraints from surrounding orogens and implications for crust-mantle decoupling. *Tectonics* 36, 3135–3154. doi:10.1002/2016tc004443

Li, X. (2015). Curvature of a geometric surface and curvature of gravity and magnetic anomalies. *Geophysics* 80, G15–G26. doi:10.1190/geo2014-0108.1

Makris, J., Egloff, F., Nicolich, R., and Rihm, R. (1999). Crustal structure from the ligurian sea to the northern apennines — a wide angle seismic transect. *Tectonophysics* 301, 305–319. doi:10.1016/S0040-1951(98)00225-X

Makris, J., Morelli, C., and Zanolla, C. (1998). The bouguer gravity map of the mediterranean sea (IBCM-G). *Boll. Geofis. Teor. Appl.* 39 (2), 79–98.

Merino, I., Prada, M., Ranero, C. R., Sallarès, V., and Calahorrano, A. (2021). The structure of the continent-ocean transition in the gulf of lions from joint refraction and reflection travel-time tomography. *J. Geophys. Res. Solid Earth* 126, e2021JB021711. doi:10.1029/2021jb021711

Morelli, C., and Nicolich, R. (1990). A cross section of the lithosphere along the european geotraverse southern segment (from the alps to Tunisia). *Tectonophysics* 176, 229–243. doi:10.1016/0040-1951(90)90268-D

Morelli, C., Pissani, M., and Gantar, C. (1975). Geophysical studies in the aegean sea and in the eastern mediterranean. *Boll. Geofis. Teor. Appl.* 18, 127–168.

Morelli, D., Locatelli, M., Corradi, N., Cianfarra, P., Crispini, L., Federico, L., et al. (2022). Morpho-structural setting of the ligurian sea: the role of structural heritage and neotectonic inversion. *J. Mar. Sci. Eng.* 10, 1176. doi:10.3390/jmse10091176

Neres, M., Neves, M. C., Custódio, S., Palano, M., Fernandes, R., Matias, L., et al. (2018). Gravitational potential energy in iberia: a driver of active deformation in high-topography regions. *J. Geophys. Res. Solid Earth* 123. doi:10.1029/2017jb015002

Nouibat, A., Stehly, L., Paul, A., Schwartz, S., Bodin, T., Dumont, T., et al. (2021). Lithospheric transdimensional ambient-noise tomography of w-europe: implications for crustal-scale geometry of the w-alps. *Geophys. J. Int.* 229, 862–879. doi:10.1093/gji/ggab520

Pašteka, R. (2006). The role of the interference polynomial in the euler deconvolution algorithm. *Boll. Geofis. Teor. Appl.* 47, 171–180.

Prada, M., Ranero, C., Sallarès, V., Zitellini, N., and Grevemeyer, I. (2016). Mantle exhumation and sequence of magmatic events in the magnaghi–vavilov basin (central tyrrhenian, Italy): new constraints from geological and geophysical observations. *Tectonophysics* 689, 133–142. doi:10.1016/j.tecto.2016.01.041

Reid, A. B., Allsop, J. M., Granser, H., Millett, A. J., and Somerton, I. W. (1990). Magnetic interpretation in three dimensions using euler deconvolution. *GEOPHYSICS* 55, 80–91. doi:10.1190/1.1442774

Roberts, A. (2001). Curvature attributes and their application to 3d interpreted horizons. *First Break* 19, 85–100. doi:10.1046/j.0263-5046.2001.00142.x

Rollet, N., Déverchère, J., Beslier, M.-O., Guennoc, P., Réhault, J.-P., Sosson, M., et al. (2002). Back arc extension, tectonic inheritance, and volcanism in the ligurian sea, western mediterranean. *Tectonics* 21, 6–23. doi:10.1029/2001TC900027

Rosenbaum, G., Lister, G. S., and Duboz, C. (2002). Reconstruction of the tectonic evolution of the western mediterranean since the oligocene. *J. Virtual Explor.* 8, 107–130. doi:10.3809/jvirtex.2002.00053

Saleh, S., and Pašteka, R. (2012). Applying the regularized derivatives approach in euler deconvolution and modeling geophysical data to estimate the deep active structures for the northern red sea rift region, Egypt. *Contributions Geophys. Geodesy* 42, 25–61. doi:10.2478/v10126-012-0003-x

Sandwell, D. T., Müller, R. D., Smith, W. H. F., Garcia, E., and Francis, R. (2014). New global marine gravity model from cryosat-2 and jason-1 reveals buried tectonic structure. *Science* 346, 65–67. doi:10.1126/science.1258213

Schettino, A., and Turco, E. (2006). Plate kinematics of the western mediterranean region during the oligocene and early miocene. *Geophys. J. Int.* 166, 1398–1423. doi:10.1111/j.1365-246x.2006.02997.x

Schmalholz, S. M., Medvedev, S., Lechmann, S. M., and Podladchikov, Y. (2014). Relationship between tectonic overpressure, deviatoric stress, driving force, isostasy and gravitational potential energy. *Geophys. J. Int.* 197, 680–696. doi:10.1093/gji/ggu040

Schmidt, S., Plonka, C., Götze, H.-J., and Lahmeyer, B. (2011). Hybrid modelling of gravity, gravity gradients and magnetic fields. *Geophys. Prospect.* 59, 1046–1051. doi:10.1111/j.1365-2478.2011.00999.x

Siravo, G., Speranza, F., and Mattei, M. (2023). Paleomagnetic evidence for pre-21 ma independent drift of south sardinia from north sardinia-corsica: "greater iberia" versus europe. *Tectonics* 42. doi:10.1029/2022tc007705

Speranza, F., Villa, I., Sagnotti, L., Florindo, F., Cosentino, D., Cipollari, P., et al. (2002). Age of the Corsica–Sardinia rotation and Liguro–Provençal Basin spreading: new paleomagnetic and Ar/Ar evidence. *Tectonophysics* 347 (4), 231–251. doi:10.1016/s0040-1951(02)00031-8

Spooner, C., Scheck-Wenderoth, M., Götze, H.-J., Ebbing, J., and Hetényi, G. (2019a). 3d gravity constrained model of density distribution across the alpine lithosphere. doi:10.5880/GFZ.4.5.2019.004

Spooner, C., Scheck-Wenderoth, M., Götze, H.-J., Ebbing, J., and Hetényi, G. (2019b). Density distribution across the alpine lithosphere constrained by 3d gravity modelling and relation to seismicity and deformation. *Solid Earth Discuss.* 10, 2073–2088. doi:10.5194/se-2019-115

Strehlau, R., Götze, H.-J., Ebbing, J., and Holzrichter, N. (2022). "Terracing and cluster analysis – new insights in potential field data prior to modelling," in *DGG 82. Jahrestagung 2022 (FID GEO)*. doi:10.23689/fidgeo-5315

Thorwart, M., Dannowski, A., Grevemeyer, I., Lange, D., Kopp, H., Petersen, F., et al. (2021). Basin inversion: reactivated rift structures in the central Ligurian sea revealed using ocean bottom seismometers. *Solid earth.* 12, 2553–2571. doi:10.5194/se-12-2553-2021

U.S. Geological Survey (2021). Earthquake Lists, Maps, and Statistics. Available at: https://www.usgs.gov/natural-hazards/earthquake-hazards/lists-maps-and-statistics (Accessed August 1, 2021).

Vigliotti, L., and Langenheim, V. (1995). When did sardinia stop rotating? new palaeomagnetic results. *Terra nova.* 7, 424–435. doi:10.1111/j.1365-3121.1995.tb00538.x

Wolf, F. N., Lange, D., Dannowski, A., Thorwart, M., Crawford, W., Wiesenberg, L., et al. (2021). 3d crustal structure of the Ligurian basin revealed by surface wave tomography using ocean bottom seismometer data. *Solid earth.* 12, 2597–2613. doi:10.5194/se-12-2597-2021

Zahorec, P., Papčo, J., Pašteka, R., Bielik, M., Bonvalot, S., Braitenberg, C., et al. (2020). The Pan-Alpine gravity database 2020. *GFZ Data Services*. doi:10.5880/fidgeo.2020.045

Zahorec, P., Papčo, J., Pašteka, R., Bielik, M., Bonvalot, S., Braitenberg, C., et al. (2021). The first pan-alpine surface-gravity database, a modern compilation that crosses frontiers. *Earth Syst. Sci. Data* 13, 2165–2209. doi:10.5194/essd-13-2165-2021